

THE PENNSYLVANIA STATE UNIVERSITY
COLLEGE OF ENGINEERING

SYSTEMS N67 16061 N67 16071
AND CONTROLS
LABORATORY

Handwritten notes:
H.C. [unclear]
A.F. [unclear]
CF-8092
cat 10

RESEARCH REPORT NO 4

UNIVERSITY PARK, PA.

OCTOBER, 1966.

THE SYSTEMS AND CONTROLS LABORATORY

C O N T E N T S

The Systems and Controls Laboratory was started in 1964 to encourage graduate research and development on engineering systems, with emphasis on improving the understanding of basic elements and devices and bridging the gap between theory and practice. The experimental equipment and facilities of this laboratory have been provided for carrying out experimental investigations on devices and systems involving many of the different engineering disciplines. Several graduate assistants are now working on projects and thesis topics of vital interest to engineers concerned with the advanced design and development of new engineering systems.

Much of the work involves mathematical and computer modeling and analysis as well as the experimental investigation of breadboard and prototype systems or devices. A major goal of this work is to accomplish a useful synthesis of analytical and experimental methods in research and development of advanced engineering systems for effective use by engineers and scientists working on future aerospace systems.

Financial support for this program is derived from the University, The Small Industries Research Program (Pennsylvania), The National Aeronautics and Space Administration, The United Aircraft Corporation, The Bendix Corporation, and The Ordnance Research Laboratory. A major share of the projects in the Systems and Controls Laboratory are carried out by graduate assistants and junior staff members under the supervision of Dr. J. L. Shearer, Rockwell Professor of Engineering, Dr. S. A. Steele, Assistant Professor of Electrical Engineering, and other members of the graduate faculty.

Hydraulic Stepping Motor	1
Spreading of Semi-Confined Jets	2
Thermal Switching of Fluidic Elements	4
Fluid Transmission Line Dynamics	4
Nonlinear System Evaluation by Observing Eigenvalue Motion	5
Application of Switching Theory to Control Systems	7
Performance of Third Order Nonlinear Control Systems	11
Size and Direction of Jets Issuing From Two-Dimensional Asymmetric Orifices	14
Characteristics of Pressure Controlled Fluid Jet Amplifiers	14
Signal Noise in Fluid Amplifiers	15
List of References	26

BLANK PAGE

HYDRAULIC STEPPING MOTOR

N67 1606

G. J. Gaskill, Graduate Assistant in M. E.

The prototype hydraulic stepping motor design, which R. W. Schiller evolved from computer simulation (2) (3)* has been constructed. The resulting device is shown in Fig. 1. At this writing the sinusoidal driving cams (3) have not been delivered, but are expected shortly. The cams are being produced on a contour following milling machine.

Experimental instrumentation has been installed to read output shaft angular velocity and position. When an actuator pressure transducer is added, it will be possible to compute the experimental drive force function. Insertion of the experimental force into the digital simulation used in design will permit a comparison of theory with experiment by simply comparing velocity vs. displacement plots.

It has been decided to use air as the working fluid in the initial testing phase, using an "air spring" device as a driver. The devices to be used

* Numbers in parentheses denote references at end.



Fig. 1 Prototype Stepping Motor

both for driving and restoring force are of the type normally used as air springs for vibration isolation.

The large effective area of the available device (approximately 10 sq. in.) gives a large displacement which results in prohibitively high demanded flow rates at cycle times near that for which the motor was designed (1/100 sec./cycle). However, the pressure needed is very low. If the potential performance of the device is to be fully realized, it will be necessary to evolve a small displacement, high pressure hydraulic actuator with no leakage. One approach to this problem is the use of a piston-cylinder arrangement utilizing a rolling diaphragm to reduce friction and sealing problems (a Bellowfram). A rolling diaphragm is a fabric membrane (polyester, glass, etc. fibers) impregnated with a rubber sealant. The use of the rolling diaphragm is indicated in Fig. 2. Two 10-gallon air-driven accumulators have been acquired for use in a power supply to provide hydraulic power for the pulse generator which will be used to drive the actuator hydraulically.

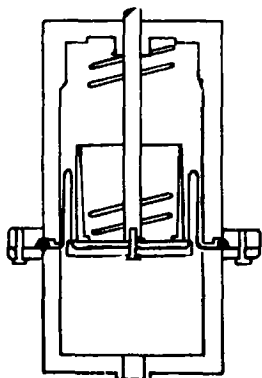


Fig. 2 Actuator with Diaphragm Seal

The effect of variation in drive force frequency was investigated with an analog computer (utilizing a sinusoidal drive force). If the stepper were to be highly sensitive to variation in this parameter, reliable operation might be difficult to achieve, and the initial "de-bugging" tests might be greatly complicated. Some analog results are shown (Fig. 3) which show reasonable response at widely varying frequencies. At frequencies under 400 rad./sec. (63 cycles/sec.) performance is erratic. It is hoped that

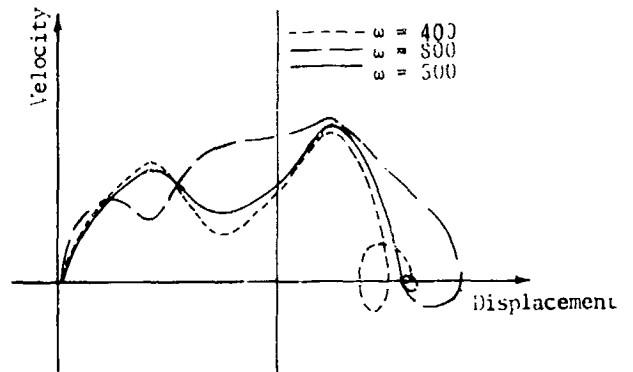


Fig. 3 One Cycle Operation at Various Drive-Force Frequencies

variations in easily manipulated parameters (such as drive force amplitude and spring constant) will enable the system to be cycled at low frequency during initial tests.

These studies are supported by NASA under Grant NGR 39-009-023.

N67 16063

SPREADING OF SEMI-CONFINED JETS

R. Bettoli, Graduate Assistant in M. E.

An experimental investigation has been performed on the effects of aspect ratio (height to width at exit plane) of a rectangular jet formed by a nozzle bounded by flat top and bottom plates and converging side walls having different profiles. Each jet is semi-confined in that it flows between the top and bottom plates after it leaves the nozzle and is allowed only to spread sideways.

The profiles employed in this investigation (shown in Fig. 4) are typical of those used in fluid amplifiers and fluid logic devices.

Most of the work was done using the round profile (a) with aspect ratios (A.R.) of 4.0, 2.0, and 1.0 obtained by varying only the nozzle width. Vertical and horizontal traverses of mean velocity (pitot static pressure) and horizontal traverses of static pressure have been measured from the outlet of the nozzle to a distance of 28 nozzle widths for A.R. = 1.0 and to a distance of 40 nozzle widths for A.R. = 2.0 and A.R. = 4.0.

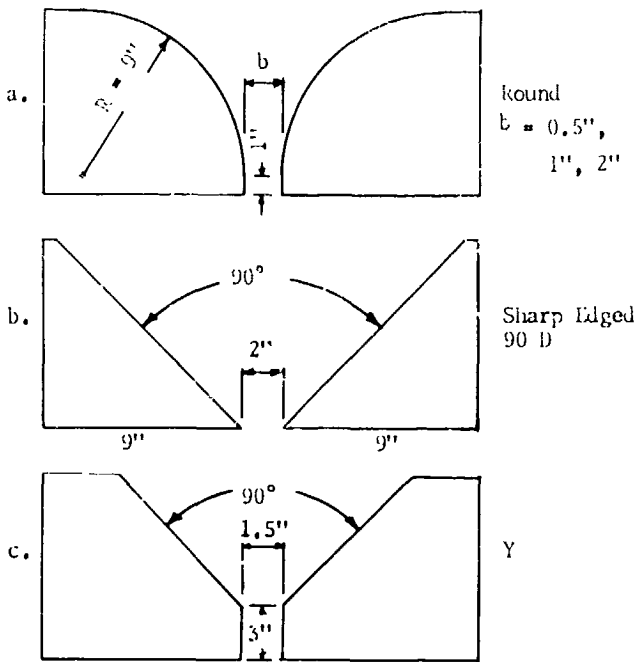


Fig. 4 Nozzle Profiles Employed

A rather uniform velocity was found all across the outlet of the nozzle for all three aspect ratios.

The vertical traverses of the mean velocity taken downstream of the nozzle exhibit a highly three-dimensional behavior of the flow. At the centerline, as one moves away from the nozzle, the velocity gradually changes from a constant profile at the nozzle to a completely developed, convex, parabolic profile with the largest velocity midway between the two plates. On one side or the other of the centerline, the profile experiences a gradual change from rectangular to concave parabolic with the lowest velocity midway between the plates, followed by a gradual transition back to an almost rectangular profile at a large distance from the nozzle.

The following features have been consistently observable with all the round profile nozzles:

1. The distance from the nozzle to where the concave shape appears does not depend on the width of the nozzle.
2. The traversal distribution of the mean velocity in a horizontal traversal midway between the top and bottom plates agrees well with the results reported for two-dimensional jets.
3. Downstream of the undisturbed core the centerline velocity is higher than that reported in the literature for the two-dimensional case and increases with decreasing aspect ratio, and the width of the jet is less than expected according to the literature.
4. The static pressures referred to a point far from the stream have shown that negative static pressures exist in most of the regions where jet spreading occurs.

5. A positive static pressure has been found only in the immediate vicinity of the outlet from the nozzle. Going downstream along the centerline, the pressure decreases to a minimum, then increases again but remains negative.

6. A relative minimum static pressure has been found at the edges of the jet outside the core. Downstream of the core, however, the static pressure increases steadily from the centerline to the edges of the jet.

For the two sharp-edged nozzles (profiles b and c) complete horizontal and vertical velocity traverses have been taken only in the region near the outlet. Centerline velocity measurements have been extended further downstream, and for the Y-shaped nozzle (profile c) total and static heads have been taken inside of the Y-shaped nozzle.

Horizontal and vertical traverse profiles similar to the ones found for the round nozzles have been found. Their magnitude and positioning, as well as the spreading of the jet, are influenced by the shape of the nozzle.

A phenomenon of "vena contracta" has been found outside the nozzle with profile b.

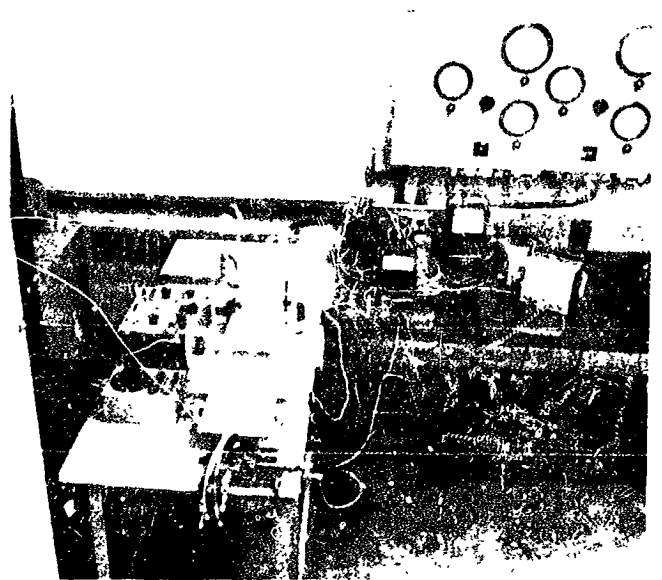
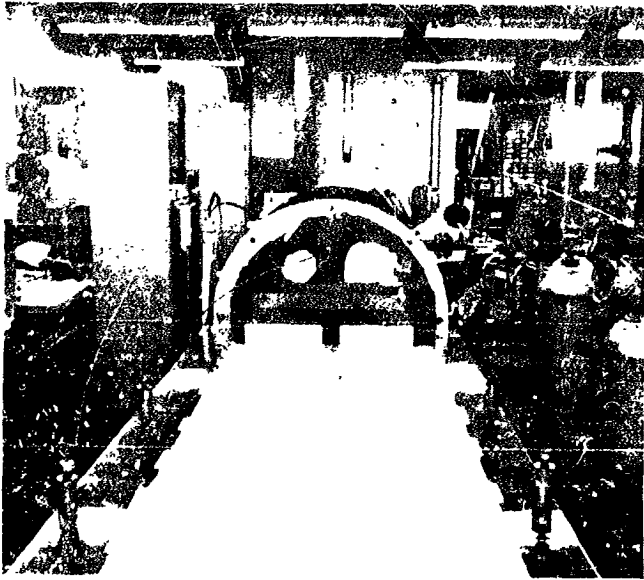
A flow detachment downstream of the inside corner of the Y-shaped nozzle has been found and the influence of the A.R. on the length of the bubble bounded by the successive reattachment has been measured for A.R. of 1.33, 0.8, and 0.57.

Photographs of the experimental apparatus are shown in Figs. 5 and 6.

This work is being supported by NASA Grant NGR 39-009-023.



Fig. 5 Photograph of Experimental Apparatus



N67 16064

Photograph of Apparatus
THERMAL SWITCHING OF FLUIDIC ELEMENTS

R. E. Tomek, Graduate Assistant in M. E.

Fig. 7 Experimental Test Setup

These studies are supported by NASA Grant
NGR 39-609-023.

The inherent high reliability of fluidics devices is due to their no-moving parts feature. This high reliability is compromised by the need for electro-mechanical switches which direct the supply of control fluid to the fluidics devices. In order to eliminate the above switches, methods are being investigated whereby the electrical signal from a computer can produce thermal fluidic switching.

The influence of a temperature field on a fluid field arises because of variation of the properties of the fluid with varying temperature. Studies by Liepmann and Fila (4) have shown the transition Reynolds Number for air flow over a flat plate decreases as the temperature of the plate increases. The influence of temperature on the separation of a fluid jet from a curved surface was investigated by McGlaughlin and Taft (5) and showed similar effects. Unfortunately, since transition is influenced also by surface roughness, acoustic noise, and by the level of turbulence, special precautions must be taken to isolate such a device from these extraneous effects. Less environmentally sensitive methods are needed.

In order to augment the influence of a temperature field, it was decided to investigate the feasibility of using a diverging channel configuration. As shown by Nikuradse (6), with increase of the adverse pressure gradient of the channel, the flow velocity gradient at the wall approaches zero. Since the influence of a temperature field on air is the same as an adverse additional pressure gradient effect, flow separation should take place at the heated wall of the diverging channel. Investigations by Moore (7), Reid (8), and Vedernikoff (9) have shown that secondary separation effects occur which are not well understood. The method of switching under study is therefore in the feasibility stage pending the outcome of preliminary experiments. A portion of the present test setup is shown in Fig. 7.

N67 16065

FLUID TRANSMISSION LINE DYNAMICS

R. G. Leonard, Instructor in M. E.

The purpose of this research is to investigate the performance of various distributed parameter components which constitute many fluid control systems and computer models for these components. The need for such models occurs in stability analyses, speed of response determinations, frequency response analyses, investigations of transient pressure surges, and in the development of schemes to suppress undesirable transient performance. These models will also facilitate the matching of transmission lines with the remainder of a fluid system.

In fabricating a computer model of a transmission line it is necessary to simulate the transport delay associated with the propagation of a pressure wave along a fluid line. Various techniques for this simulation, including an extensive treatment of the Padé approximation, were discussed by Herritt (10). It was decided that a digital technique would be utilized to accomplish the delay simulation for this investigation. The equipment has been designed and is currently being installed. A schematic diagram of the system is shown in Fig. 8, and a photograph is included as Fig. 9. The analog voltage is first converted to a binary signal which is then progressively shifted through the delay units, in which both the number of shifts and the rate at which the shifts occur can be varied to obtain the required time delay. After the delay is obtained the signal is converted to an analog signal. When completed, this equipment will be a versatile addition to the existing data acquisition facilities of the Systems and Controls Lab. and will add some digital capability to the existing Dynamics Simulation Labs. analog computation equipment.

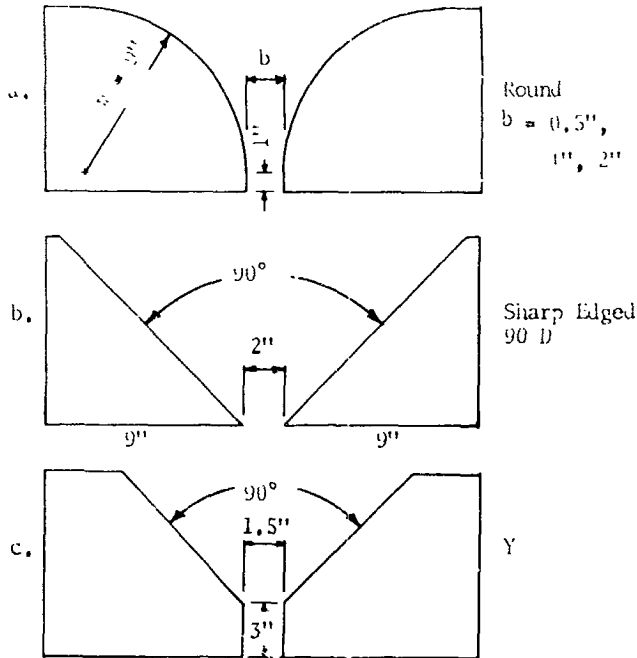


Fig. 4 Nozzle Profiles Employed

A rather uniform velocity was found all across the outlet of the nozzle for all three aspect ratios.

The vertical traverses of the mean velocity taken downstream of the nozzle exhibit a highly three-dimensional behavior of the flow. At the centerline, as one moves away from the nozzle, the velocity gradually changes from a constant profile at the nozzle to a completely developed, convex, parabolic profile with the largest velocity midway between the two plates. On one side or the other of the centerline, the profile experiences a gradual change from rectangular to concave parabolic with the lowest velocity midway between the plates, followed by a gradual transition back to an almost rectangular profile at a large distance from the nozzle.

The following features have been consistently observable with all the round profile nozzles:

1. The distance from the nozzle to where the concave shape appears does not depend on the width of the nozzle.
2. The traversal distribution of the mean velocity in a horizontal traversal midway between the top and bottom plates agrees well with the results reported for two-dimensional jets.
3. Downstream of the undisturbed core the centerline velocity is higher than that reported in the literature for the two-dimensional case and increases with decreasing aspect ratio, and the width of the jet is less than expected according to the literature.
4. The static pressures referred to a point far from the stream have shown that negative static pressures exist in most of the regions where jet spreading occurs.

5. A positive static pressure has been found only in the immediate vicinity of the outlet from the nozzle. Going downstream along the centerline, the pressure decreases to a minimum, then increases again but remains negative.

6. A relative minimum static pressure has been found at the edges of the jet outside the core. Downstream of the core, however, the static pressure increases steadily from the centerline to the edges of the jet.

For the two sharp-edged nozzles (profiles b and c) complete horizontal and vertical velocity traverses have been taken only in the region near the outlet. Centerline velocity measurements have been extended further downstream, and for the Y-shaped nozzle (profile c) total and static heads have been taken inside of the Y-shaped nozzle.

Horizontal and vertical traverse profiles similar to the ones found for the round nozzles have been found. Their magnitude and positioning, as well as the spreading of the jet, are influenced by the shape of the nozzle.

A phenomenon of "vena contracta" has been found outside the nozzle with profile b.

A flow detachment downstream of the inside corner of the Y-shaped nozzle has been found and the influence of the A.R. on the length of the bubble bounded by the successive reattachment has been measured for A.R. of 1.33, 0.8, and 0.57.

Photographs of the experimental apparatus are shown in Figs. 5 and 6.

This work is being supported by NASA Grant NGR 39-009-023.



Fig. 5 Photograph of Experimental Apparatus

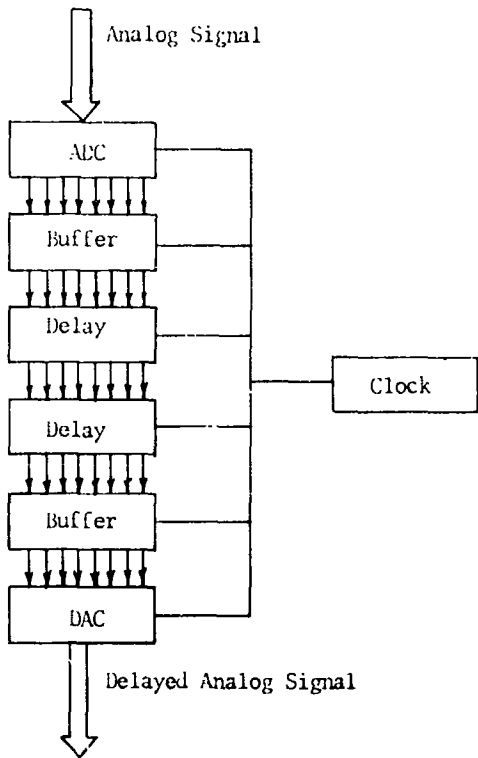


Fig. 8 Schematic of Delay Simulator



Fig. 9 Delay Simulator

The mathematical and computer models will be verified by comparison with fluid lines constructed in the Systems and Controls Laboratory and lines a control loops already in existence in industry.

Some theoretical aspects of fluid transmission lines were given by Raizada (2). Other significant works in the field have been given in references (12), and (13).

This work is being supported by Small Industry Research Grant 00669.

N67 16066

NONLINEAR SYSTEM EVALUATION BY
OBSERVING EIGENVALUE MOTION

S. A. Steele, Assistant Professor in E. E.

The question is often asked, "How much can the roots (eigenvalues) of the pseudo-characteristic equation (3) of a nonlinear system vary during transient response and still give approximate but useful information in the analysis?" Strictly speaking, the root concept is useful only in linear systems. However, some efforts which have been made to extend the concept to nonlinear cases have been successful. The stability techniques of Liapunov have been used to develop a generalized Routh-Hurwitz criterion applicable to certain types of systems (18). Determination of whether a given nonlinear system response will be oscillatory or aperiodic has been accomplished for second-order systems by observing root excursions (14) (17). Although such a determination involves approximations, the results have been consistently good when compared to the results of computer solutions. It is the extension of this root excursion method to higher order problems that is the major interest here. Recently, excellent results have been obtained with third-order systems. Therefore, the emphasis here is on higher order systems such as fourth and seventh.

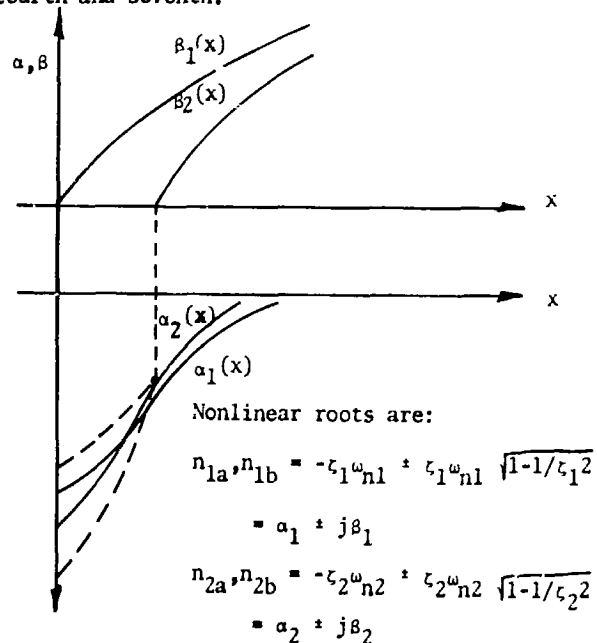


Fig. 10 Root Excursion Plot for a Fourth Order System
Observe a possible fourth-order root excursion plot in Fig. 10. This plot was obtained from the following type of system differential equation for $t > 0$:

$$[D^4 + f_1(x)D^3 + f_2(x)D^2 + f_3(x)D + f_4(x)] x = 0$$

where

$$x(0+) = k$$

$$x(0-) = 0$$

For systems of this type with complex roots having nearly equal α terms, it is shown by Wasta (15) that for no overshoot

$$\int_k^0 \beta_1(x)dx + \int_k^0 \beta_2(x)dx + \int_k^0 \alpha_1(x)dx \geq 0 \quad (1)$$

Note that in this case the integrand of $\alpha_1(x)$ could have been $\alpha_2(x)$ or $(\alpha_1 + \alpha_2)/2$.

This is consistent with the previous arguments used in developing root excursion methods (14) (17). The sum of the integrals involving $\beta_1(x)$ and $\beta_2(x)$ represents the energy to be dissipated if no overshoot is to occur. Therefore, only one of the real roots is used to represent the energy loss term, $\alpha(x)$.

In the above case where $\alpha_1 \approx \alpha_2$, Eq. (1) constituted a necessary and sufficient condition. However, if $\alpha_1 \neq \alpha_2$, it is necessary to use the smallest of α_1 and α_2 as the integrand, and Eq. (1) then constitutes a sufficient condition. For instance, k may be larger and Eq. (1) may not be satisfied, but still no overshoot will occur. This can be demonstrated by several examples.

Given:

$\dot{x}_1 = x_2$	Initial conditions at $t = 0$:
$\dot{x}_2 = x_3$	$x_1 = k$
$\dot{x}_3 = x_4$	$x_2, x_3, \dots, x_7 = 0$
$\dot{x}_4 = x_5$	
$\dot{x}_5 = x_6$	
$\dot{x}_6 = x_7$	
$\dot{x}_7 = -28x_7 - 322x_6 - 1960x_5 - 6769x_4 - 13,132x_3$	
	$- 13,068x_2 - 5040x_1 - 5040 x_1 x_1$

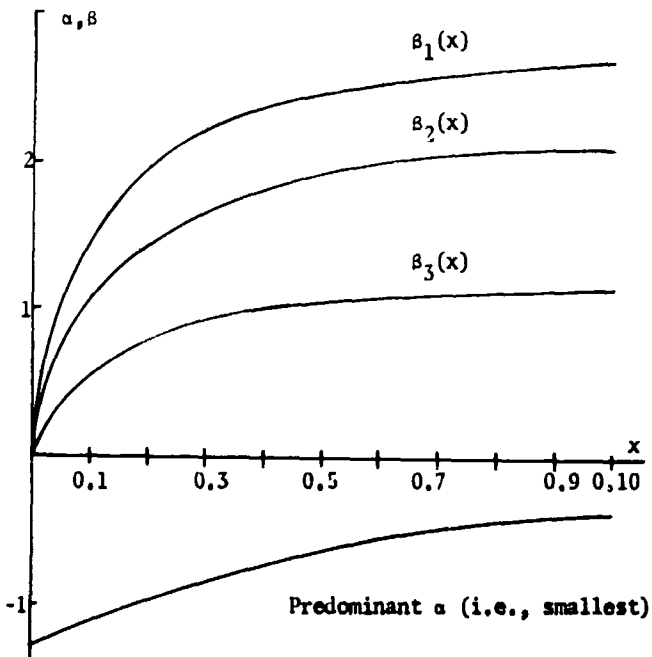


Fig. 11 Root Excursion Plot for Seventh Order System

The root plots are in Fig. 11. The sufficient condition indicates no overshoot for $k = 0.15$. However, there is also no overshoot at $k = 0.2$. Finally at $k = 0.3$ a small amount of overshoot occurs, and at $k = 0.5$ there is 7% overshoot.

If we next modify the nonlinearity so the system now has

$$\dot{x}_7 = -28x_7 - 322x_6 - 1960x_5 - 6769x_4 - 13,132x_3 - 13,068x_2 - 5040x_1 - 504|x_1|x_1,$$

the root excursion plots are shown in Fig. 12. The sufficient condition indicates no overshoot at $k = 0.3$, but actually no overshoot occurs until k is greater than 1.5. In this case the sufficiency condition would be too pessimistic for useful application, but it is interesting to note that the effect of the nonlinearity is weaker than in the previous example.

Because of the inadequacy of the above method in some cases, it may be better to use another method. This would involve transforming the original system into a set of decoupled second-order systems. Then each decoupled second-order part could be analyzed separately. This may give better results. Let us see how this could be carried out for a fourth-order system. Using vector matrix notation:

$$\ddot{\vec{x}} = \underline{A}\dot{\vec{x}} + \underline{B}\vec{x}$$

\underline{A} and \underline{B} are square matrices which take on different values as \vec{x} (dependent variable) changes. These are obtained in the same way as the root excursions of second-order systems. The nonlinear system is frozen at each point as \vec{x} changes, and a set of values for \underline{A} and \underline{B} are obtained at each point.

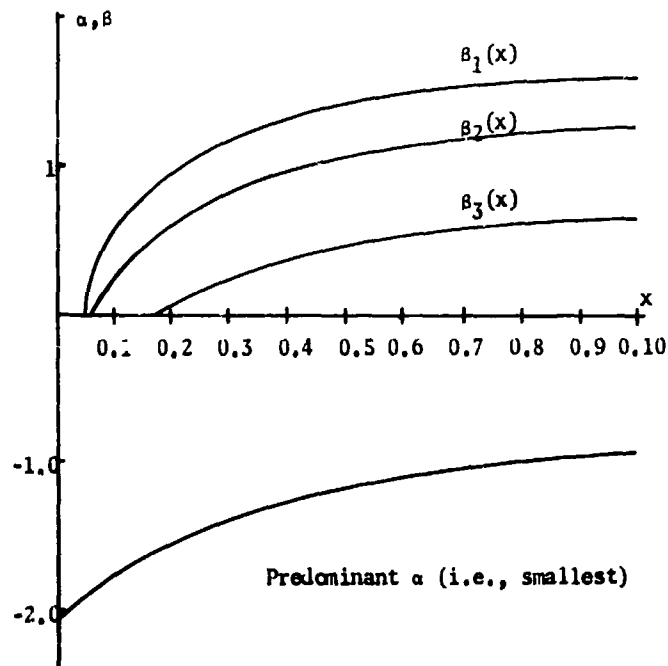


Fig. 12 Root Excursion Plot for Modified Seventh Order System

To decouple the system A and B must be diagonalized (16).

Let

$$\underline{x} = \underline{R}y$$

Then

$$\ddot{\underline{y}} = \underline{R}^{-1}\underline{A}\underline{R}\dot{\underline{y}} + \underline{R}^{-1}\underline{B}\underline{R}y$$

If \underline{R} is formed by independent invariant vectors of matrix \underline{A} , $\underline{R}^{-1}\underline{A}\underline{R}$ will be diagonalized with the eigenvalues of \underline{A} along the diagonal.

Let

$$\underline{R}^{-1}\underline{A}\underline{R} = \underline{W}, \quad \underline{R}^{-1}\underline{B}\underline{R} = \underline{Z}$$

$$\ddot{\underline{y}} = \underline{W}\dot{\underline{y}} + \underline{Z}y$$

Now diagonalize \underline{Z} .

Let

$$\underline{y} = \underline{G}\phi$$

$$\ddot{\underline{\phi}} = \underline{W}\dot{\underline{\phi}} + \underline{G}^{-1}\underline{Z}\underline{G}\underline{\phi}$$

If \underline{G} is formed by independent invariant vectors of matrix \underline{Z} , $\underline{G}^{-1}\underline{Z}\underline{G}$ will be diagonalized with the eigenvalues of \underline{Z} along the diagonal.

Let

$$\underline{G}^{-1}\underline{Z}\underline{G} = \underline{\psi}$$

Now

$$\ddot{\underline{\phi}} = \underline{W}\dot{\underline{\phi}} + \underline{\psi}\underline{\phi}$$

or

$$\ddot{\phi}_1 = W_{11}\dot{\phi}_1 + \psi_{11}\phi_1$$

$$\ddot{\phi}_2 = W_{22}\dot{\phi}_2 + \psi_{22}\phi_2$$

The roots of these uncoupled second-order systems may be displayed; and as x changes, a root excursion plot is possible. The basic requirement for no overshoot may be applied to each second-order system. Care must be taken in this method since ϕ_1 and ϕ_2 could exhibit individually no overshoot; but when transformed back through the transformation matrices \underline{R} and \underline{G} respectively, overshoot could occur. This cannot happen if \underline{R} and \underline{G} have only positive coefficients. In practice, the system could be evaluated in a decoupled mode and the results (value of dependent variable for which no overshoot occurs) could be transformed back to the original form. Therefore, not many transformations are required. Obviously a digital computer must be used to carry out this procedure, but it may be faster than brute force solution of the original differential equations using Runge-Kutta or faster subroutines. The major time-consuming step would be finding the eigenvalues of the \underline{A} and \underline{Z} matrices, since they must be found at all the desired points as x moves. A simple method of finding eigenvalues such as Linn's Method requires a good bit of time when roots are close together. On a sixth-order

example attempted on the Electrical Engineering Department's computer and finding eigenvalues at ten points, the necessary calculations took four times longer than a Runge-Kutta general solution. This was also verified approximately on the IBM 7074 at the University's Computation Center. Inverting matrices and other control functions are quite fast. There should be a more optimum method of obtaining roots than used here.

However, one advantage of this technique is the better "feel" for sensitivity that the designer may obtain when operating with decoupled systems. If it is clear which equation or equations (decoupled) is causing the overshoot effect, then as parameters are varied, the effect may be predicted. This is especially true if the transformation matrices have positive coefficients.

In general, it is quite possible at this time to use root excursion methods on higher order systems if sufficient conditions for no overshoot are desired. To analyze the system the method can be tedious as when using the roots of a high order linear system. It is quite possible that a main advantage of this method would be a shorter computational time on a computer. This is extremely important for real time studies. This means that the technique used for obtaining roots must be quite optimum and converge quite quickly to a value with appropriate accuracy. It would seem that this could be done faster than a procedure to actually solve the equation. The normal programs available at this time did not operate in this manner.

This work has been supported by NASA Grant NGR 39-009-023.

N67 16017

N67 16067

APPLICATION OF SWITCHING THEORY
TO CONTROL SYSTEMS ✓

S. A. Steele, Assistant Professor of E. E.

As more and more control systems become of a digital nature, the control engineer requires a mathematical background in this area. This involves an understanding and application of Boolean algebra and techniques of function simplification that in the past has found large scale application in the design of digital computers. This branch of mathematics, often referred to as switching theory, normally uses set theory notation. The two major branches of analysis are combinational and sequential. In a combinational system the output is continuously a function of the input, while in a sequential system the output is a function of the previous input as the system "sequences" along in a prescribed manner. A digital controller for a control system involves circuitry of a combinational and sequential type. A very simple type of digital controller was shown by Raizada (25).

However, when the system designer attempts to apply the general theory, he finds it is not flexible enough to consider all of his variables. Observing large scale digital computer designs he finds a good bit of "seat of the pants" methods being applied. In general, switching theory is not easily responsive to hardware restrictions. This is particularly evident in integrated circuits. The number of components may not be as important as the number of inputs because

of excessive wiring problems. The purpose of this report is to present the author's method of obtaining an important part of the digital system design where the more complicated standard methods require excessive time and more mathematical background.

The problem of minimizing the number of internal states in a sequential network is of prime importance and has been discussed extensively in the literature (19,20,23). However, all known methods require some enumeration and search techniques to finally arrive with the minimum number of states. Some of these methods are quite sophisticated but tedious. Here we will present a method whereby a good minimization of states occurs so that generally the minimum number of states is obtained. The time required to apply this method is quite short.

A state table is made up from the words of the designer and indicates what should happen when a particular input is present. A typical table is shown in Fig. 13. If the system is in state 1 when input combination i_1 occurs, the system will go to state 3 (next state) and give an output of 0. Some of the next states and/or outputs are "don't cares" (the designer does not care). The presence of "don't cares" can help considerably in simplifying the table. To save equipment, it is usually important to combine equal states in order to obtain the minimized state table. However, Ginsburg (24) has shown that using all possible fixed combinations for the "don't cares" and then attempting to find states that are equal in order to simplify the table will not always result in the simplest state table. This is because some of the "don't care" next states should be changed during the simplification process in order to use the full effect of a "don't care" condition.

Some basic definitions which will be useful in the following discussion are given below:

1. Two internal states q_i and q_j of a state table are compatible if, and only if, for all input sequences the

Internal States	Input Combination			
	i_1		i_2	
	Next State	Output	Next State	Output
q_1	3	0	-	-
q_2	4	0	3	0
q_3	-	-	5	1
q_4	-	-	6	0
q_5	6	0	6	-
q_6	-	-	-	-

Fig. 13 State Table for Example #1

output sequence which results when the table is initially in q_i is the same output sequence which results when the table is initially in q_j whenever both outputs are specified.

2. A collection of compatible sets (where a set consists of two or more states) is closed if, and only if, for each set the next states under a particular input are in the same set.
3. A state table is covered by a collection of sets if, and only if, all of the original states occur in the sets.
4. A maximum compatible collection of sets is formed if, when the original state is added to the sets of the collection, an incompatible set results somewhere in the collection.

The technique is to find sets of compatible states and then form a maximum compatible collection of sets which is closed. This is normally not the simplest number of states. Then subsets of this maximum compatible collection are found by some method (enumeration, trial and error) to form a collection which is closed and covered and will reproduce the sequence of the original table. This can be demonstrated by attempting to simplify the state table in Fig. 13. A compatibility table is shown in Fig. 14, from which a maximum compatible collection may be obtained in a systematic way. For example, the table indicates that states 5 and 6 are always compatible, but states 2 and 4 are only compatible if states 3 and 6 are compatible. In Fig. 14 the procedure is as follows (23):

1. List the pairs of states which are shown to be compatible in the right-most column of the table for which any such pairs exist.

2	3, 4 x				
3	✓	x			
4	✓	3, 6	x		
5	3, 6	4, 6 3, 6	5, 6	✓	
6	✓	✓	✓	✓	✓
	1	2	3	4	5

✓ indicates compatible states.
x indicates incompatible states.

Fig. 14 Compatibility Table for Example #1

- Proceed to the next column to the left. If the state to which this column corresponds is compatible with all members of a previously determined set, add this state to the set. If the state is not compatible with all members of a set but is compatible with a subset, form a new set including the current state and subset. List any compatible pairs which are not included in any already determined set. Do not retain any sets which are subsets of other sets. Repeat until all columns of the compatibility table have been considered.

For Fig. 14 this process will result in the following sequence of sets (21).

{56}
 {456}
 {456}, {356}
 {2456}, {356}
 {2456}, {1356}, {1456} - maximum compatible collection

By trial and error and considering subsets of the maximum compatible collection, the following closed collection of two sets may be obtained: {12456} and {1356}. In general, this collection of sets is not unique. Therefore, the table may be reduced to two new states. It is our purpose to eliminate the trial and error aspect of this procedure and proceed directly to a minimum table.

The procedure outlined by the following steps and demonstrated by the following examples tends to eliminate trial and error:

- Find maximum compatible collection.
- Group the next states of the maximum compatible collection together into new sets. If the state table is not covered, add the required states to make up new sets.
- Take the union of these sets. Do not allow unions which form sets with incompatible states*.
- In (3) starting in the set containing the most states, form a class (which is covered) with the minimum number of sets. Check to see if the collection is closed.
- If after (4) the state table is not covered, go back to the sets in (2) and add the minimum number of these sets to cover the table. Now check to see if the addition is closed. If the collection does not close, add the next set with the most states.
- In (2) to insure closure, it is quite possible that a collection will contain one set with only one state (or a subset of the sets in (2)). Keep this in mind when trying to close the collection of sets.

* If after (3) the resulting collection of sets is a maximum compatible collection, nothing has been gained by this procedure. If simplification is possible, subsets will be required.

Example 1

Let us apply this to the table in Fig. 13.

- {2456}, {1356}, {1456}
- {46}, {36}, {56}, {12}
- {2456}, {1356}
- {2456}, {1356} This is a closed collection.

Example 2

Observe the state table in Fig. 15.

- {45}, {236}, {34}, {126}, {14}
- {16}, {45}, {34}, {26}, {12}
- {126}
- Go to Step 5.
- {126}, {34}, {45} This is a closed collection.

Internal States	Input Combination					
	i ₁		i ₂		i ₃	
	Next State	Output	Next State	Output	Next State	Output
q ₁	3	0	-	-	2	-
q ₂	-	-	4	0	6	-
q ₃	5	1	-	-	-	0
q ₄	-	-	1	1	1	-
q ₅	1	-	-	-	6	-
q ₆	4	-	5	-	6	-

Fig. 15 State Table for Example #2

Example 3

Observe the state table in Fig. 16. This example has been done by an excellent theoretical technique, but is quite tedious and long (19).

- {cfg}, {deh}, {abde}, {bcd}, {ag}
- {cd}, {he}, {gf}, {ab}, {de}, {ad}, {eb}, {ae}, {ag}
- {abde}, {hed}
- Go to Step 5. {abde}, {hed}, {gf}, {cd} This is not closed. Go to Step 6.
- {abde}, {hed}, {gf}, {c} This is a closed collection.

Internal States	Input Combination													
	i ₁		i ₂		i ₃		i ₄		i ₅		i ₆		i ₇	
	Next State	Output	Next State	Output	Next State	Output	Next State	Output	Next State	Output	Next State	Output	Next State	Output
q _a	a	0	-	-	d	0	e	1	b	0	a	-	-	-
q _b	b	0	d	1	a	-	-	-	a	-	a	1	-	-
q _c	b	0	d	1	a	1	-	-	-	-	-	-	g	0
q _d	-	-	e	-	-	-	b	-	b	0	-	-	a	-
q _e	-	-	e	-	a	-	-	-	b	-	e	-	a	1
q _f	b	0	c	-	-	1	h	1	f	1	g	0	-	-
q _g	-	-	c	1	-	-	e	1	-	-	g	0	f	0
q _h	a	1	e	0	d	1	b	0	b	-	e	-	a	1

Fig. 16 State Table for Example #5

More than a dozen examples have been done using the aforementioned procedure. While it is not completely straightforward in all cases, it does tell the user which way to turn. One may ask, "Why not use a computer with a basic search technique to obtain the minimum number of states?" The computer programs are generally not efficient for all types of state tables, and in control problems the number of states in the original problem is not always great. If there are many states, the concept of "divide and conquer" is used to form more than one state table but with not many states. Therefore, it is helpful to have some rules to follow in attaining an equivalent state table with many states removed. To help judge in difficult problems, a minimum bound (21) can be determined so that the designer knows there can be no fewer states than the bound. This is obtained by determining the maximum incompatible collection* and interpreting this to find out at least how many states are required.

In order to show how a state table can be formed for a real world problem, let us look at a simple example that will lead to the state table in Fig. 13. A device in a plant is to observe two lights, and when the lights operate in a particular sequence a function is to be performed. This function is the opening and closing of a circuit breaker (switch). The over-all system has two characteristics. Both lights will never be on at the same time, and when a light comes on it is on for a predetermined amount of time. There are three sequences that must be followed by the device in question. In the first sequence which must start in state 1, when light a comes on the switch must be opened. Then if light b operates (comes on), the switch must be closed. Now if light a operates, the switch must be opened. However, if instead of light a light b operates, it then makes no difference if the switch is opened or closed. From now on, regardless of which of the lights operates, the switch may be opened or closed.

* This collection is formed by building up incompatible sets until a point is reached where adding another original state to a set makes it compatible.

Another sequence must also be followed which must start in state 2. If light a operates, the switch must be opened. Then if light b operates, the switch must be left open. Then, regardless of the operation of the lights, the switch may be open or closed.

The third sequence must also start in state 2. If light b operates, the switch must be opened. Then if light b operates again, the switch must be closed. Then if light a operates, the switch must stay closed. However, if light b has operated instead of light a, the switch may be either open or closed. From now on, regardless of which lights operate, the switch may be opened or closed.

Any combinations which have not been discussed cannot occur in the system. The desired device can have six internal states to remember the proper sequence as in Fig. 13. However, because some of the sequences have common properties, the number of internal states can be reduced as indicated previously. This eliminates a good deal of equipment. The inputs i₁ (light a) and i₂ (light b) indicate when a light operates. Whether the switch is closed or open is indicated by the output 0 (open) or 1 (closed). Refer to Fig. 13.

Many of the fundamental techniques employed in the application of switching theory to large complex systems (such as digital computers) are not convenient for use in the design of control systems. The techniques described here have been developed to simplify the use of switching theory in this type of problem. This procedure may be used with any switching system.

N67 16068
 PERFORMANCE OF THIRD ORDER
 NONLINEAR CONTROL SYSTEMS

R. Wasta, Graduate Assistant in E. E.

This report examines a method of predicting the step response of control systems described by third-order nonlinear differential equations. The nonlinearities are specified mainly as being smooth and not a function of the derivatives of the dependent variable.

The method is based on the construction of a root excursion plot, which is the locus in a root vs. dependent variable plane of the roots of a nonlinear characteristic equation.

Comments are made on the various possible shapes of third-order root excursion plots and the step response of the system is related to each particular shape. In particular, it is shown that for certain third-order root excursion plots, it is possible to predict the exact value of system gain or step amplitude which will yield the fastest possible no-overshoot response.

Advantages of the method are mainly that the number and location of the nonlinearities are not limited. The prediction of the response is not restricted to a small range immediately around an equilibrium point. That is, for the cases in which the method does apply, if the system is stable over an extended range, the point of the fastest no-overshoot response within that range can be predicted very accurately. Presently there are no other methods available which will yield response information of this type.

A possible extension of the method to higher-order nonlinear systems is demonstrated by a fourth-order example.

Examples

A. Third-Order Systems

In Fig. 17 is shown a block diagram of a control system with the nonlinear element $f(e) = e^2$. The pseudo-characteristic equation for this system is

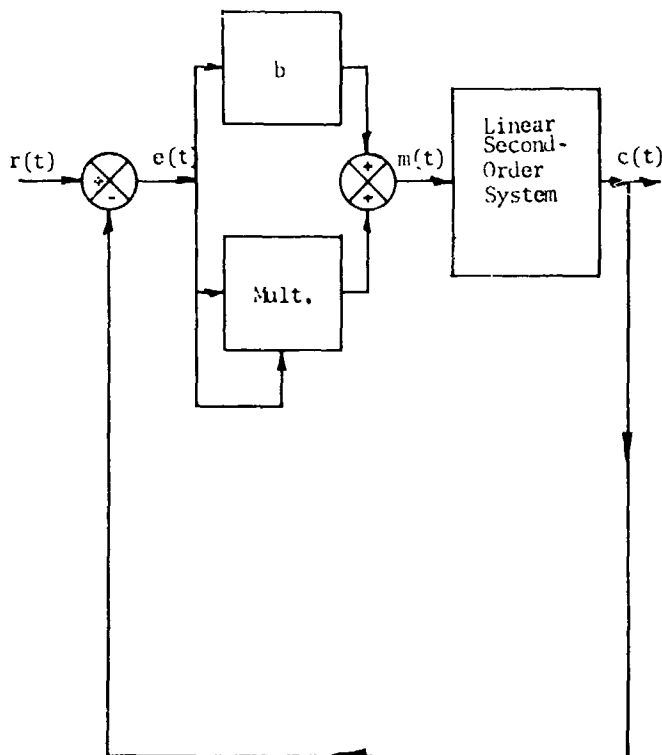
$$a_3s^3 + a_2s^2 + a_1s + (d + e) = 0 \quad (1)$$

The roots n of this nonlinear system, found from Eq. (1), are shown as functions of e in Fig. 18. This plot is constructed by solving for the roots of Eq. (1) which result when successive values of e are substituted in it, and then plotting these roots vs. e .

It can be noted that in the time responses shown in Fig. 19 the optimum no-overshoot response of the particular system described by Eq. (2) occurs with

$$s^3 + 3s^2 + 3s + (1 + e) = 0 \quad (2)$$

* The name "pseudo-characteristic equation" is used here to denote the type of characteristic equation used by Volz (26). It is not the same as the characteristic equation obtained from linearizing the system equations.



$$m(t) = (b + e)e(t)$$

$$(a_3D^3 + a_2D^2 + a_1D)c(t) = m(t)$$

Fig. 17 Block Diagram of Third-Order Nonlinear System

an $e(0+)$ of 1.0. This value can be very accurately predicted from an examination of the root plots of Fig. 18. It is seen that the cross-hatched area between the real part loci for n_2, n_3 and the e -axis from $e = 0$ to $e = 1.0$ is equal to the corresponding area between the imaginary part locus n_2 , (or n_3) and the e -axis.

This point of fastest no-overshoot response can be predicted in like manner for all systems which have root excursion plots which satisfy the several requirements outlined later.

For values of $e(0+)$ in which the $\text{Im}[n]$ area is greater than the $\text{Re}[n]$ area (e.g., at $e(0+)$ of 1.2 in Fig. 19), the response will be oscillatory. (Curve [1] in Fig. 19). When the $\text{Re}[n]$ area is the greater (e.g., $e(0+)$ of 0.8), a slower aperiodic response results.

B. Fourth-Order Systems

In Fig. 20 is shown the root excursion plots for a nonlinear system having the pseudo-characteristic equation, Eq. (3). Here it is necessary that the real part loci be relatively close to each other as in Fig. 20.

$$[s^2 + (2 - e)s + (1 + 3)] [s^2 + 2s/(1 + e^2) + 1] = 0 \quad (3)$$

BLANK PAGE

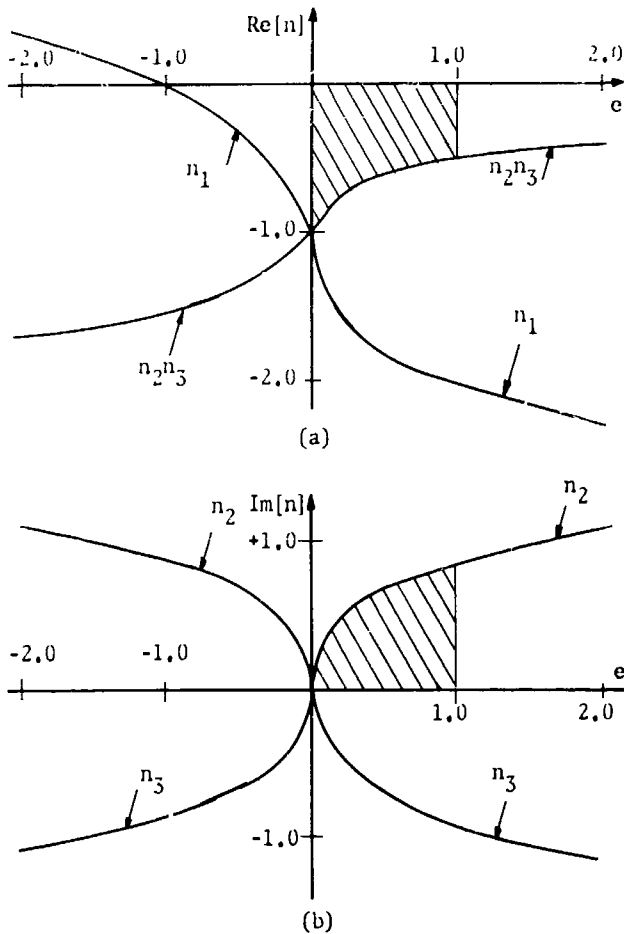
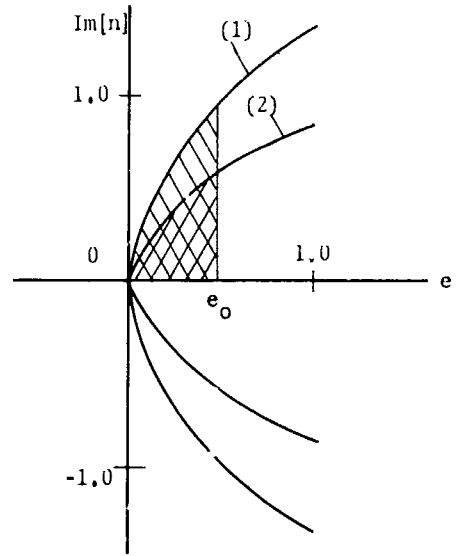


Fig. 18 Root Excursion Plots for System with Pseudo-Characteristic Equation:
 $s^3 + 3s^2 + 3s + (1 + e) = 0$



Point of fastest no-overshoot response occurs when sum of cross-hatched areas in $Im[n]$ equals the cross-hatched area under the most positive $Re[n]$ plot (at about $e(0) = 0.49$).

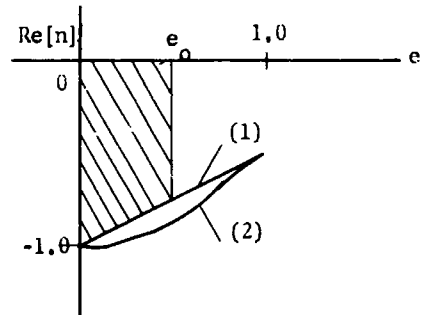


Fig. 20 Root Excursion Plots for System with Pseudo-Characteristic Equation:
 $[s^2 + (2 - e)s + (1 + e)] [s^2 + 2s/(1 + e^2) + 1] = 0$

The point of fastest no-overshoot response is then predicted by determining the value of $e(0+)$ such that the sum of the two $Im[n]$ areas from $e = e(0+)$ to $e = 0$ is equal to the $Re[n]$ area over the same range of the most positive $Re[n]$ locus (Curve [1]). A number of different examples which were worked out using this criterion proved to be very accurate in predicting the initial condition for response with no overshoot.

Requirements for Application

A. General

1. The nonlinear differential equation which describes the physical system must be converted to an autonomous differential equation by suitable choice of dependent variable.
2. The nonlinearities must be smooth and must not involve derivatives of the dependent variable.

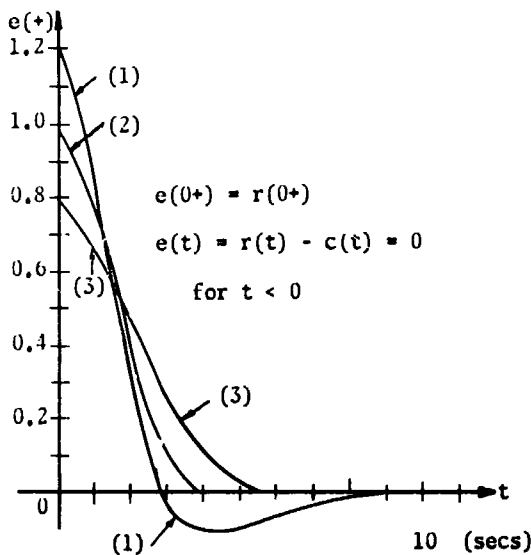


Fig. 19 Analog Computer Simulation of Response of System of Fig. 17 to step changes in $r(t)$.

3. Generally, the drive signal is a step input. This restriction results primarily from aforementioned requirements (1) and (2). A limited class of ramp forcing functions can be made to satisfy requirements (1) and (2) by differentiation of the describing equation. In general, however, the differentiation results in nonlinear derivatives of the dependent variable.
4. The stability of the system must be guaranteed in the range under consideration.

Satisfying the above requirements will make possible the formulation of a pseudo-characteristic equation whose roots are used to construct the root excursion plots of the nonlinear equation.

B. Specific

5. In the root excursion plot, the imaginary-part locus must go through the origin.
6. The real-part loci associated with the remaining quadratic factor must have a positive, or at least zero, slope.
7. For third-order systems, the always-real root locus must have (a) a negative slope, or (b) if it has a zero or positive slope, the locus must be equal to, or more negative than, the remaining real-part locus.
8. For fourth-order systems, if the roots exist in the form of two complex-conjugate pairs, the two sets of real-part loci must lie relatively close to each other.

Outline of Procedure to be Used in Analyzing Third-Order Systems

The first step in the procedure of analyzing a nonlinear control system by the root excursion method is to determine the pseudo-characteristic equation of the nonlinear equation. The second step is the construction of root excursion plots from this equation. Examination of the root excursion plots is then undertaken to determine if it is possible to accurately predict the response of the system.

If the root excursion plot shows the imaginary-part locus to be zero at least at the origin, the step response of the system can be predicted with an accuracy which is generally dependent on the position and slope of the real-part loci.

The prime requirement of the real-part loci is that the loci associated with the quadratic factors must have a positive, or at least a zero, slope. If this requirement is met, the next is that the remaining always-real locus must have a negative slope, or if it has a zero or positive slope, the locus must be equal to, or more negative than, the remaining real root loci.

If the real-part loci have the proper location and slope as just described, then the point of fastest no-overshoot step response can be very accurately determined by locating the value of the independent variable at which the areas under the imaginary-part plot and real-part plot of the quadratic factor are equal.

In those cases where the imaginary-part is not zero at the origin, it is not possible to determine the exact point of the fastest no-overshoot response. The general procedure in these cases is then to make a slight parameter change in the system and to note how the pseudo-characteristic equation, and hence the root excursion plot, is affected. In some cases this procedure will result in the imaginary-part going to zero at the origin of the plot and the analysis can be undertaken as outlined above to determine the optimum response. If the change in parameter does not cause the root excursion plot to become zero at least at the origin, an accurate prediction cannot be made; but by noting the general change in the shape of the plot, some response information may be inferred. For example, if a parameter change causes the imaginary area to decrease, a less oscillatory response could be expected.

As has been mentioned above, the plotting of the root excursion loci is a necessary step in system analysis by this method. A brief summary of some observations made during this work can be helpful in constructing these plots and giving some idea beforehand of the general shape of the plots. A summary of results according to the location of the nonlinear term is now presented.

Consider pseudo-characteristic equations of the type

$$I) [s^3 + a_2s^2 + a_1s + f_0(x)] = 0 \quad (4)$$

For stable equations of this type, the always-real root will always lie between $f_0(x)$ and the dependent-variable axis. Hence, if $f_0(x)$ is plotted on the root excursion plane, some idea is given as to the position and slope of the always-real root. This is especially true when the plot of $f_0(x)$ is near the dependent-variable axis.

If the inequality

$$(a_1 - q_2)^2 > 12a_2f_0(x) \quad (5)$$

is not true at an equilibrium point (a value of x for which $f_0(x) = 0$), then an imaginary-part exists at that point. This information is useful because the equilibrium point of interest is usually at the origin of the root excursion plot and the optimum no-overshoot response cannot be predicted from plots of this type. Inequality, Eq. (5), is only sufficient, however, and it is possible for imaginary-parts to exist when the inequality is true.

It was also noted that if questions concerning system stability are to be avoided, the nonlinear term $f_0(x)$ should be restricted to a range so that $a_1a_2 > f_0(x)$ is true throughout the range. Eq. (4) could result from a control system with a nonlinear gain element. An equation which has nonlinearities in the damping and gain terms could result from a system which

has a transport delay. This type of equation is next considered.

$$\text{II) } [s^3 + a_2s^2 + f_1(x)s + f_0(x)] = 0 \quad (6)$$

If the nonlinearities $f_1(x)$ and $f_0(x)$ of Eq. 6 can be related by

$$\frac{f_0(x)}{c} + ac = f_1(x), \quad (7)$$

the term $(a + c)$ can be calculated. If $(a + c) = a_2$, a zero-slope always-real locus equal to $-c$ will exist and the method of analysis will apply. If $(a + c) > a_2$, the slope of the quadratic real-part loci will be negative, which is incorrect for analysis by this method. If $(a + c) < a_2$, the imaginary-part plot in general will not be zero at the origin, and accurate response predictions are not possible. Hence, relation (7) can be used in cases like Eq. (6) to get an idea of the probable root plots.

The general third-order nonlinear equation is next considered.

$$\text{III) } [s^3 + f_2(x)s^2 + f_1(x)s + f_0(x)] = 0 \quad (8)$$

In this case, if $f_c(x)$ denoted the equation of the always-real root on a root excursion plot, it was noted that a stable system will generally have the term $[f_2(x) - f_c(x)]$ positive. This indicates that the $f_c(x)$ plot will always lie between the $f_2(x)$ plot and the dependent-variable axis. Hence, a plot of $f_c(x)$ on the root excursion plot, combined with the observation in 1) that $f_c(x)$ tends to follow the slope of $f_0(x)$ in stable systems, will give useful information on the probable slope of the always-real locus, $f_c(x)$.

This work is being done under Exploratory and Foundational support from Penn State's Ordnance Research Laboratory.

the effects of fluid viscosity and entrainment of surrounding fluid were ignored. Results from this analysis compared well with some experiments that had been carried out earlier using a Schlieren light system to show up the jet edges.

A second phase of this work involved extending the method of force defect coefficients to the case of asymmetric pressure conditions in the region surrounding the issuing jet. This involved carrying out a relaxation solution in the holograph plane, using a digital computer. In twenty complete cycles of computation the relaxation method seemed to be converging on a reasonably good answer. Additional work is required to determine conclusively how effective this method will be.

A technical paper is being prepared by Dr. Begg at the University of Glasgow to describe this work in more detail.

This work is an extension of some of his own doctoral thesis research (30) at the University of Glasgow.

N67 16069 ✓

SIZE AND DIRECTION OF JETS ISSUING FROM
TWO-DIMENSIONAL ASYMMETRIC ORIFICES

J. L. Shearer, Rockwell Professor of Engineering
(for Dr. R. D. Begg)

During his working visit of six months at The Pennsylvania State University as a postdoctoral research associate, Dr. R. D. Begg, of the University of Glasgow, extended his earlier work on fluid jets. He helped provide guidance to Mr. Bettoli's experimental investigation (see write-up by Bettoli in this report), and he carried forward some interesting ideas on the computation of the boundaries of unsymmetric two-dimensional jets. This latter work involved the extension of earlier work by Von Mises (27), Jobson (28), and Bragg (29).

One phase of this work employed the method of force defect coefficients in determining size and direction of ideal jets issuing from asymmetric orifices into a region of uniform pressure. Both compressible and incompressible flows were studied, but

N67 16070 ✓

CHARACTERISTICS OF PRESSURE CONTROLLED
FLUID JET AMPLIFIERS

A. K. Stiffler, Graduate Assistant in M. E.

Static Characteristics

The previous work carried out by the writer on knife edge type amplifiers included a study of the static characteristics of a device of a particular design. This study was warranted because preliminary findings differed considerably from the results of Simson's analysis of similar amplifiers (31). A synopsis of the conclusions was given in Research Report No. 3 (3). The reader is referred to two reports, (32) (33), for a complete presentation of the experimental results.

These results differed from Simson's in two important aspects. Gains were about three times higher, and quiescent control flows were about twice as large as predicted by Simson. In this amplifier, knife edge location had been changed to accommodate what appeared to be faster free jet spreading of the power jet. At the time, the only factor to which these discrepancies could be attributed was the relatively small aspect ratio (ratio of nozzle height to width). A value of unity was used in this design. Subsequently, an experimental investigation of the effect of aspect ratio on jet spreading has been carried out by R. Bettoli (pp. 2-3). His conclusions are that the aspect ratio has little effect on free jet profiles midway between the top and bottom plates, although some distortion occurs at these boundaries. However, there are strong indications that flow separation does occur within the nozzle when an abrupt change exists in the nozzle wall angles.

The nozzle of the experimental amplifier was changed from its abrupt-angle converging section to a more rounded configuration (Fig. 21). Some quick experiments were made, and the device performed in better agreement with Simson's results. A program is now under way to investigate the effect of nozzle design, in conjunction with low aspect ratios, on the free jet profile.

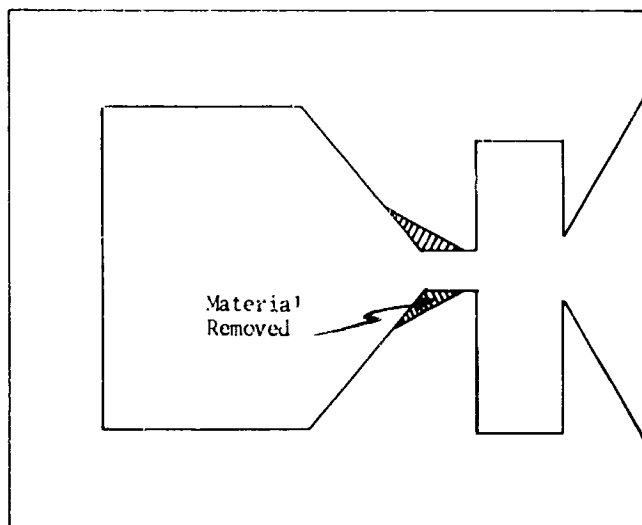


Fig. 21 Profile of Nozzle and Control Port Section of Experimental Fluid Amplifier (Approx. 4x Size)

It is now possible to quantify and predict static performance of knife edge amplifiers having large aspect ratios, based upon knowledge of two-dimensional jet spreading. However, it is very difficult to fabricate the deep passages needed to assure two-dimensional flow. Therefore, the flow patterns of the spreading jet from a low aspect ratio nozzle are three-dimensional and rather complex. For this reason there does not seem to be much to be gained in a systematic "black box" testing of large numbers of amplifiers. The main hope of quantifying amplifier performance seems to lie in gaining a better understanding of these three-dimensional flow phenomena and how they are affected by nozzle geometry and knife-edge or wall location.

Dynamic Characteristics

Although fluid amplifiers seem to offer a number of advantages for fluid system design, there have not been many applications developed as yet. The reason is contained in the apparent difficulty of obtaining appropriate predictable models for system analysis based on understanding of key flow phenomenon and geometrical characteristics. The author's recent investigation of static characteristics has helped to emphasize the need for better modeling capability (33). The problems involved with obtaining dynamic models of fluid amplifiers are considerably greater. Static modeling provides a start, at least, with pressure-flow curves which can be determined experimentally to verify the adequacy of the model and specify actual capability.

There have been some recent efforts to model fluid amplifier dynamics. In general, the amplifier is thought to have three distinct parts. One is concerned with how the input portion reacts as the load impedance on some driving source. The signal effect is then transferred to the receivers by way of the jet. The output portion then serves as a source for driving a load or another amplifier. Proceeding with

the aforementioned outline, Belsterling (34) and Boothe (35) have approached the modeling of momentum control amplifiers as shown schematically in Fig. 22.

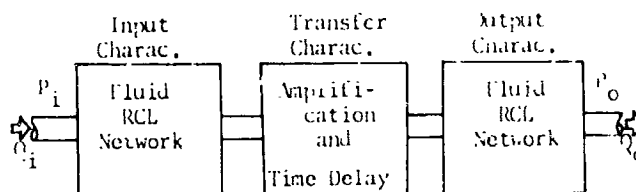


Fig. 22 Schematic Diagram for Model of Momentum Control Amplifiers

Specific RCL networks were employed which seemed to model their amplifiers well at frequencies up to 1,000 cps. Gurski (36) studied the dynamics in the control port region of a pressure controlled amplifier. He developed a simplified dynamic model for a single control port and unconfined jet. The only jet deflection studied was that which resulted from port interaction with an attached transmission line during resonance.

These contributions to the dynamics problem have been important first steps. However, the approach of (34) and (35) is limited to modeling for responses to sinusoidal disturbances of small amplitude. Also, the circuits apparently were chosen arbitrarily, and there is some question of their ability to predict size and shape effects. Gurski's work (36) was confined to the study of the dynamic interaction of a single control port and jet. The nature of the excitation probably produced very small jet oscillations. In all cases, no reference was made to supply flow variations resulting from mean control pressure changes and to possible feedback between receivers and control ports from load variations.

In addition there is neglect of the phenomena known as edgetones (37) (38) in dynamic modeling. A jet striking an edge produces a time variant force on the jet which is related to the shedding of the vortices. When the jet assumes a wavy shape, it is modeled as a continuous elastic media. This causes some doubt about pure time delay representations of the jet. The relation of edgetones to amplifier noise is now being carried out in the Systems and Controls Laboratory by J. C. Tamulis.

This work on fluid amplifiers is sponsored in part by the Hamilton Standard Div. of United Aircraft Corp., Hartford, Conn., and in part by NASA Grant NGR 39-009-023.

N67 16071

SIGNAL NOISE IN FLUID AMPLIFIERS ✓

J. C. Tamulis, Graduate Student in M. E.

Work has continued on the investigation of basic sources of noise in fluid amplifiers. Background information and prior results can be found in previous SCL Research Reports (1, 2, 3). A more complete presentation of data, results, and conclusions will be included in a doctoral thesis which is now being written. Additional information concerning this thesis can be obtained from the Director, Systems and Controls Laboratory, The Pennsylvania State University.

Digital Data Results of Digital Data Processing Scheme
(Power Density Spectra)

In Research Report No. 3 (3) some preliminary results obtained through use of the digital data processing scheme were presented. Figs. 23, 24, 25, and 26 of this report are the power density spectra obtained digitally for the autocorrelation curves shown in Figs. 18 and 17 respectively of Research Report No. 3. As previously mentioned, the pressure signal noise is narrow band; i.e., it is clustered into narrow bands of the total frequency range investigated. From inspection of the figures and consideration of the lengths of the passages under test (see Research Report No. 3), it is indicated that the passages could be considered as "organ pipes" with appropriate boundary conditions. If the boundary conditions for the passages are taken to be,

1. Completely blocked at the sensed end
2. Completely open at the end interacting with the power jet,

then the resonant frequencies are predicted by odd multiples of the velocity of sound divided by four times the passage length.

$$f_n = \frac{nc}{4L} \quad \text{where } n = 1, 3, 5, 7 \dots \quad (1)$$

Use of this expression implies certain assumptions, one of which involves making an end correction to the length "L". The end correction for the control port passages is the most difficult to make because of the complex geometry which exists at each end. The end correction for a simple unflanged organ pipe, open at one end, was calculated by Rayleigh (42) to be 0.6R where "R" is the radius of the tube.

The corrected length found for the cylindrical receivers located as shown in Fig. 20 of Research Report No. 3 was 5.75 in., the open end correction being

negligible compared to the 0.25 in. existing in the adapter used to connect the pressure transducers. For the single receiver shown in Fig. 19 of Research Report No. 3, the transducer was mounted flush at the blocked end and the open end correction was 0.30 in., giving a corrected length of 42.3 in.

Using these lengths and 13,500 in./sec. for c, the fundamental frequencies predicted by (1) for the 5.75 in. and 42.3 in. receivers are 587 cps and 79 cps respectively. These values compare well with the results of Figs. 24 and 25, considering the resolution of the measuring schemes. The value of "L" for the control ports was somewhat arbitrarily taken to be 5.0 in. which gives a predicted fundamental frequency of 675 cps which corresponds to the highest frequency spike shown in Fig. 23. Fig. 23 also shows two other spikes in the spectrum. The lowest frequency spike at approximately 100 cps was found to be due to reflections caused by the plumbing associated with supplying and monitoring pressure at the control ports. By a more judicious selection of fittings and tube sizes, this spike was largely eliminated. However, the intermediate spike remained. In order to isolate passage resonance from possible dynamic interaction effects with the power jet, an acoustical test of the amplifier geometry of Fig. 20 of Research Report No. 3 was made. In this test the receiver geometry was removed and the power jet and control flows were shut off. A loudspeaker driven with a white noise generator was positioned in proximity with the fluid amplifier and used to excite the control port passages as shown in Fig. 27. The control port pressure was sensed with a Kistler pressure transducer located as shown and the pressure signal spectrum at this point was recorded using an electronic frequency analyzer. This yields a spectrum of average pressure amplitude for point A versus frequency as shown in Fig. 28, which shows that the spectrum does indeed peak at about 700 cps and that there is an additional acoustical resonance at around 450 cps. The spectrum shown in the photograph was obtained by taking a thirty-second time exposure. This procedure was followed in order to obtain an averaging effect for the spectrum envelope.

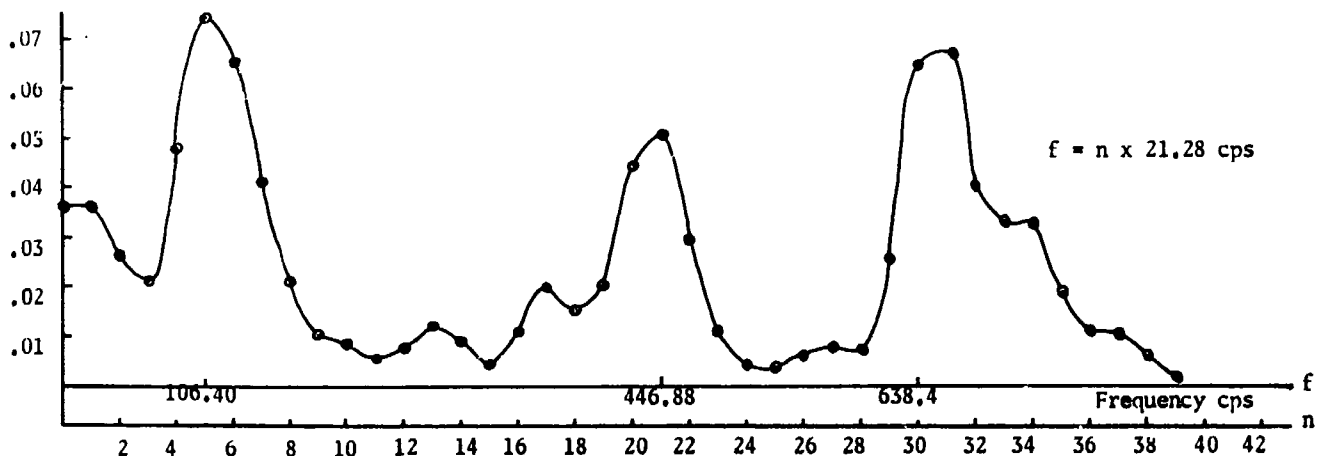


Fig. 23 Power Density (Spectral Distribution) -- Differential Pressure In. Differential Pressure Measured at Extremities of Control Ports.

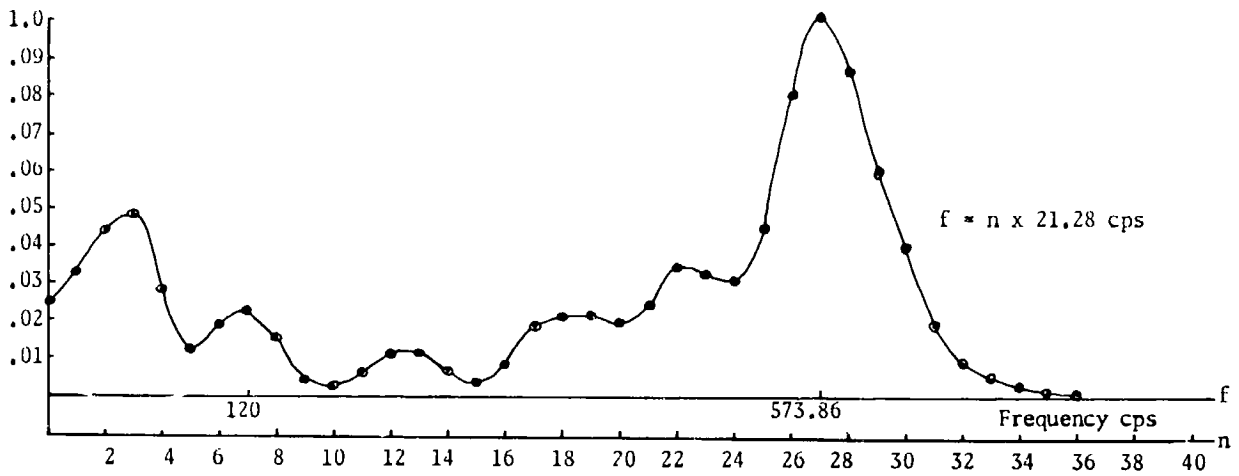


Fig. 24 Power Density Spectrum of Differential Pressure Measured at Load End of Blocked Receivers

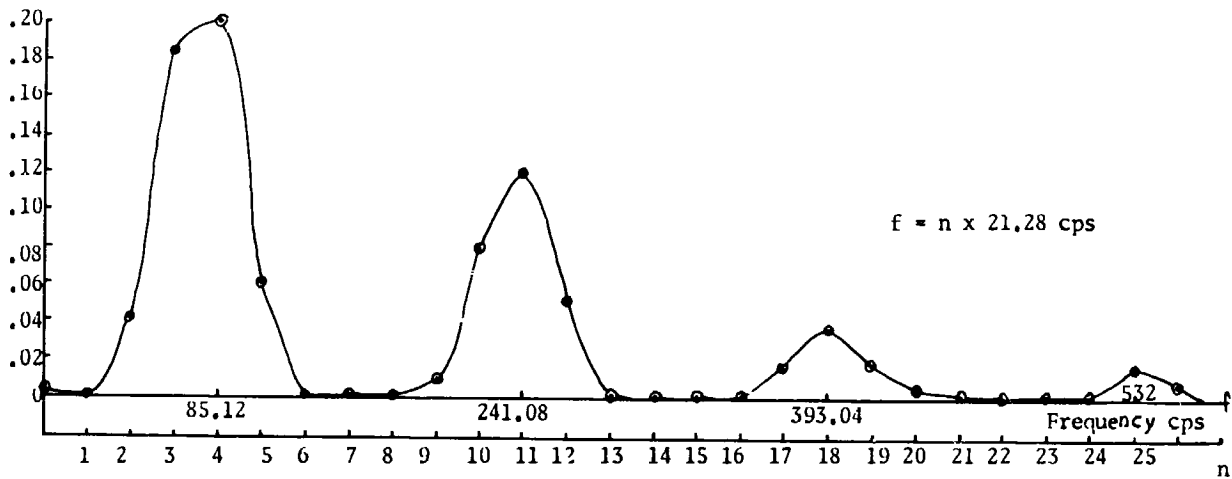


Fig. 25 Power Density Spectrum for Pressure Measured at Load End of Single Block Receiving Tube

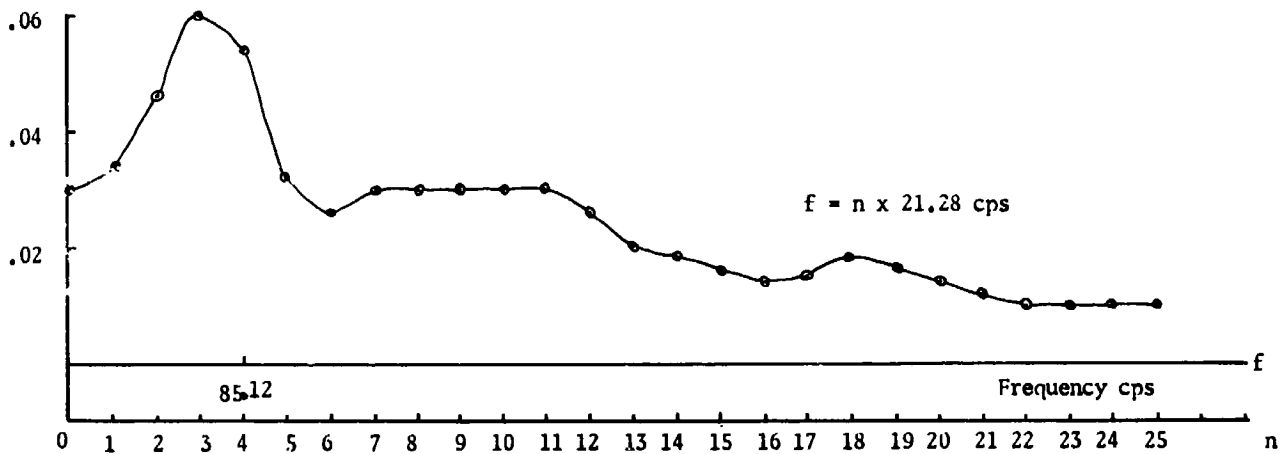


Fig. 26 Power Density Spectrum of Fluctuating Velocity at Point Near the Entrance of a Single Receiver Concentric with Jet

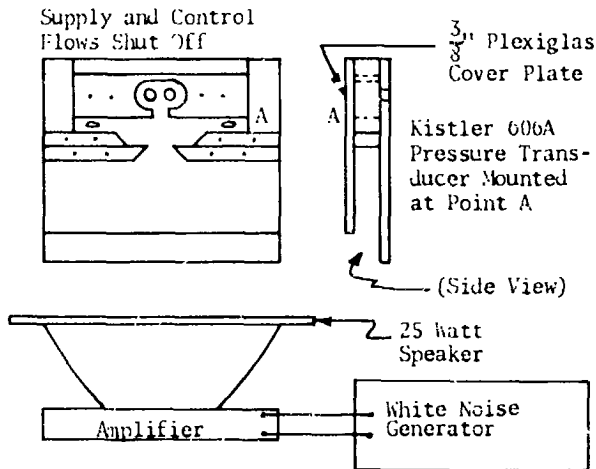


Fig. 27 Schematic Diagram of Acoustic Test Set-Up Using Loudspeaker

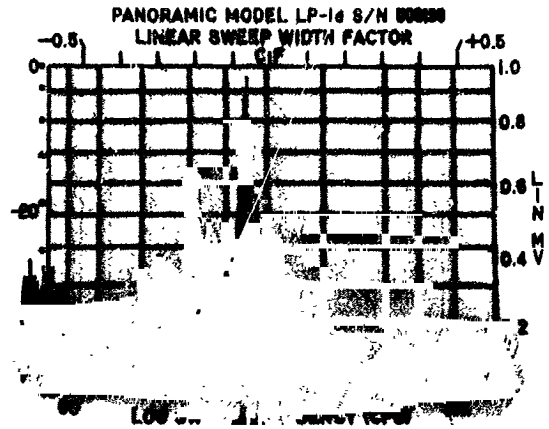


Fig. 28 Results of Acoustical Test

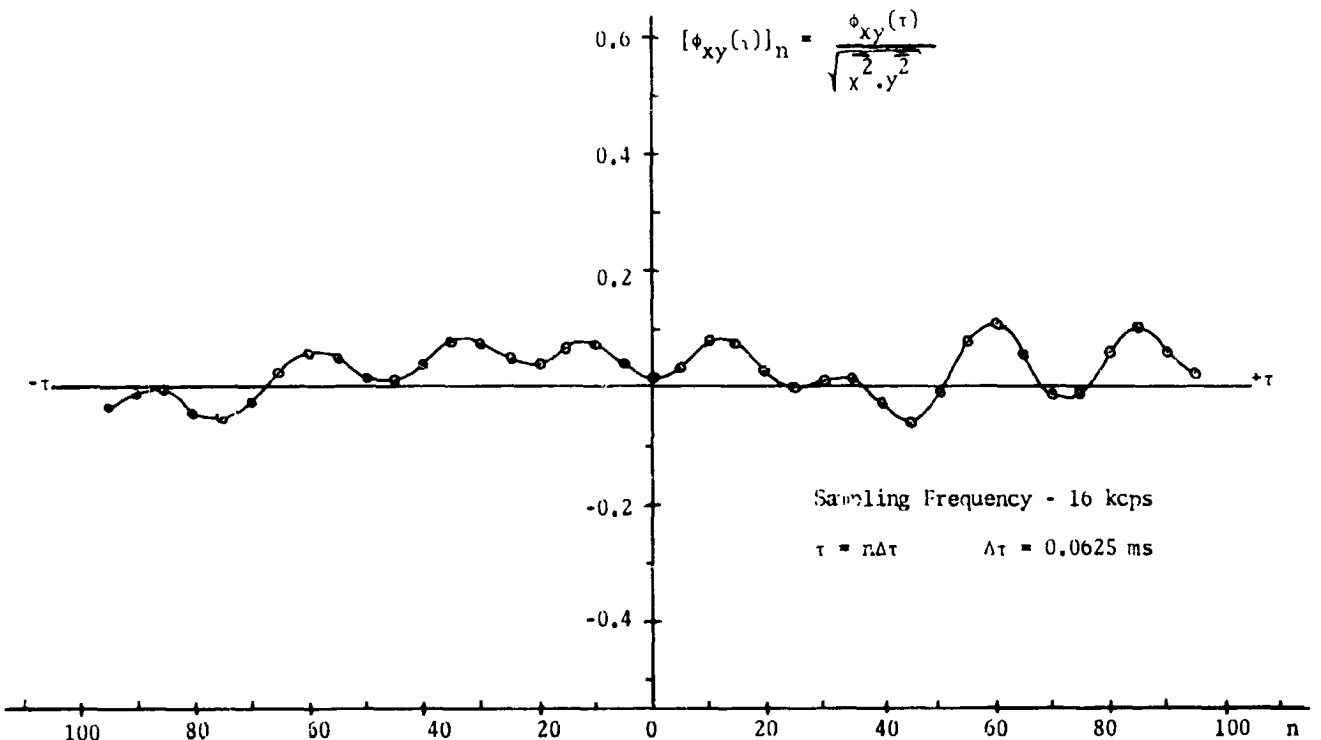


Fig. 29 Normalized Crosscorrelation Function Between Input Differential Pressure $x(t)$ and Output Differential Pressure $y(t)$

Digital Results of Processed Data (Crosscorrelation)

As indicated in Research Report No. 3 (3), there appeared to be negligible correlation between the input and output differential pressure measurements for the amplifier tested. Fig. 29 shows the computer crosscorrelation function for the two signals whose spectra are shown in Figs. 23 and 24 (autocorrelations shown in Fig. 18 of Research Report No. 3). There is insignificant crosscorrelation between them. Figs. 23 and 24 give an indication of why this is so. The figures show the two signals to have peaks at completely unrelated frequencies.

Conclusions - Digital Scheme

Results of the above tests and later results caused a reassessment of the usefulness of the digital scheme. It was concluded that while the scheme

was working satisfactorily, it was not the most efficient way to collect data for this investigation. The scheme was too time consuming, too expensive, and not accurate enough considering costs for the type of data under investigation. The analog scheme outlined in Research Report No. 3 (3) was relatively fast, accurate, and inexpensive.

Jet Dynamics

The results for the fluid amplifier geometry analyzed by the digital scheme tend to obscure some basic phenomena. Also, the model was difficult to probe and instrument. Attention was turned to the simpler geometry represented by Fig. 30. The larger nozzle (3 in. x 1 in.) mentioned in earlier reports was now used and it was confined between two plates in order to simulate fluid amplifier conditions. A photograph of this model is shown in Fig. 31.

A series of tests were run with this larger model, varying H , Y , and V_0 . The geometry was made unsymmetrical (solid lines) or symmetrical (dotted lines) as shown in Fig. 30. Numerous spectra of the type shown in Fig. 32 were obtained. A number of spikes were

found to be present not predicted by expression (1). Further investigation brought out the fact that these spikes were caused by dynamic interactions at the knife edge explainable through the use of ideas developed by Curle and Powell (39) (38) to discuss edgetones.

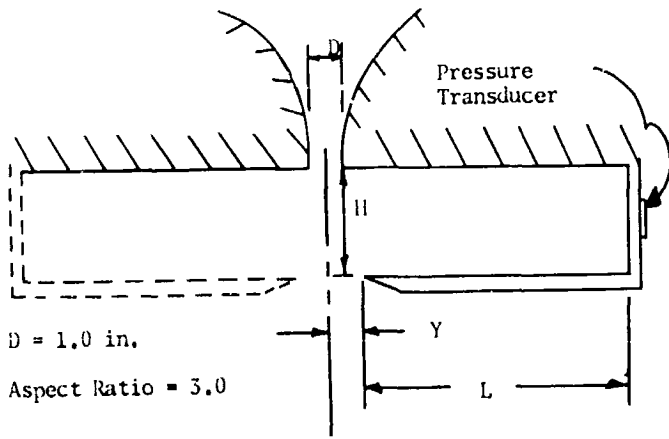


Fig. 30 Geometry of Test Set-Up with Large Nozzle for Study of Jet-Knife Edge Resonance

Fig. 31 Large Test Model

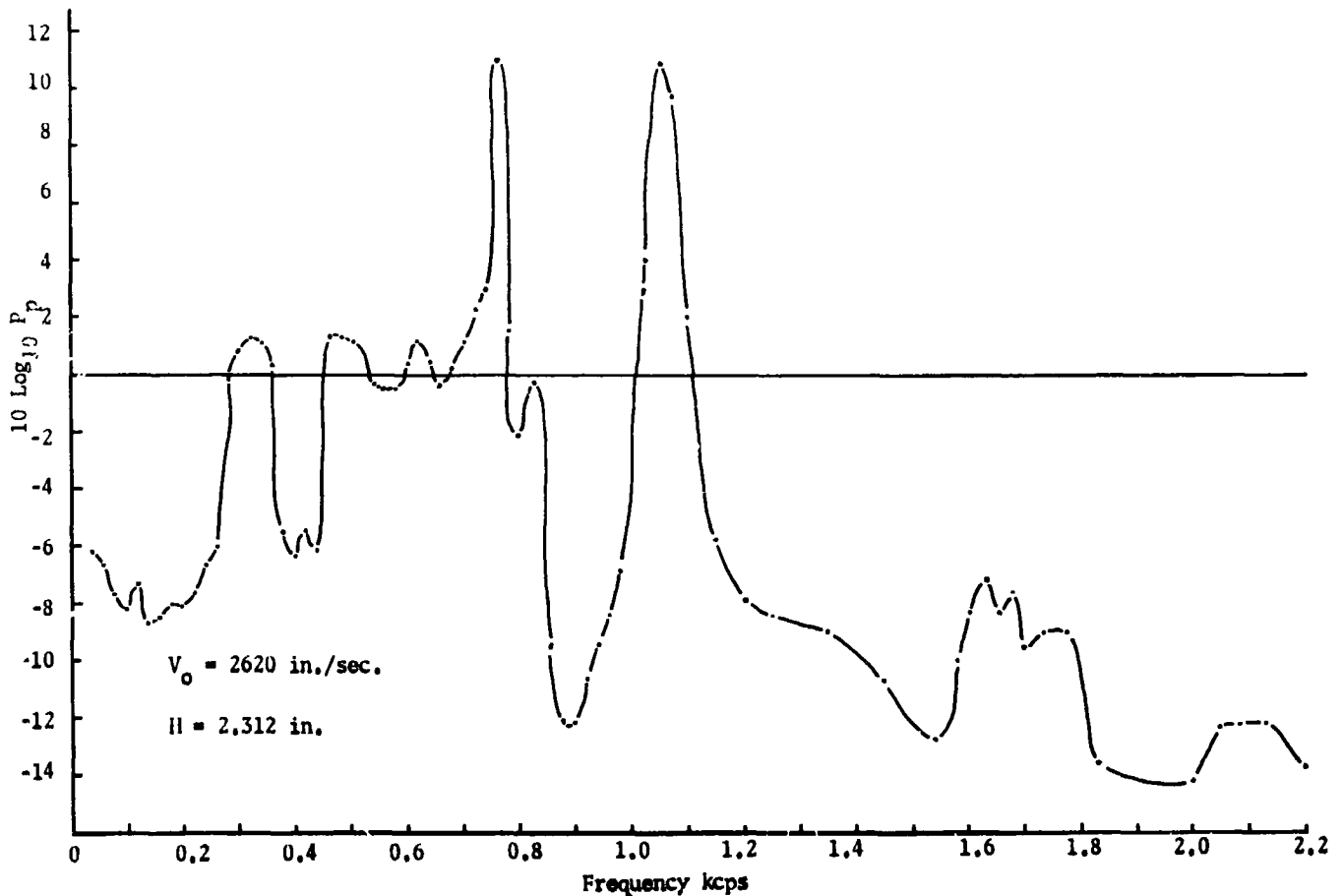


Fig. 32 Power Density Spectrum of Pressure Transducer Signal

Fig. 33 schematically depicts a vortex model of the jet and knife edge configuration of the type found in some amplifier designs. In addition to the alternating right-hand and left-hand vortices formed in the mixing region at the edges of the spreading jet (which occur in a random way even when no knife edge is present), there is a series of moving vortices of varying strength formed just inside the knife edge due to a "peeling off" of some of the varying lateral jet momentum by the knife edge. Consideration of the vortex pattern shown along the jet and the "peel-back" vortex formed by the knife edge inducing a transverse feed-back flow near the nozzle, leads to the following expression for predicting certain frequencies of jet-knife edge resonance (edge normal to jet):

$$f_m = mf_d \quad \text{where } m = 3, 7, 11, 15, \text{ etc.} \quad (2)$$

and

$$f_d = 1/2 \frac{V_0}{4H}$$

V_0 = nozzle exit plane velocity of jet

A corresponding simplified expression based on References (39) and (38) for the more usual case (edge parallel with jet) is:

$$f_m = mf_d \quad \text{where } m = 1, 5, 9, 13, \text{ etc.} \quad (3)$$

Table I is a collection of some results obtained from some of the extensive experiments with Fig. 30. Column VI shows that there is a predominance of values

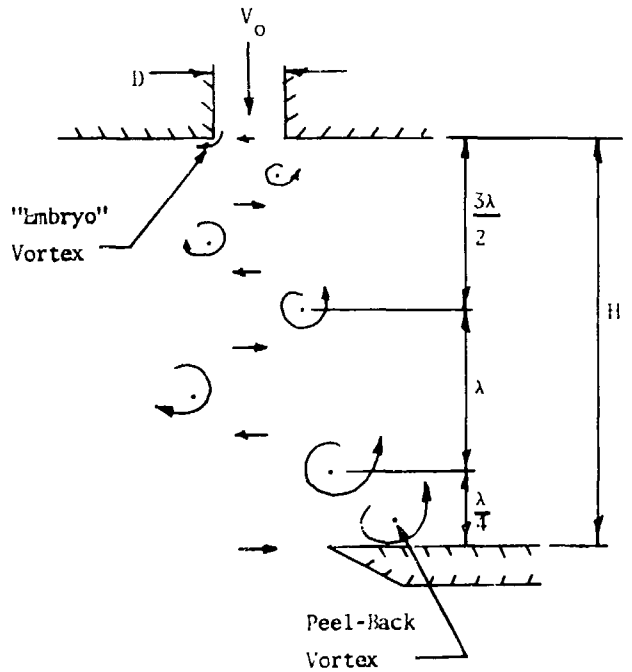


Fig. 33 Jet-Knife Edge Vortex Model

for "m" = 3 and 7. The knife edge vortex model mentioned previously is only rather qualitative, and efforts have been made to develop a more detailed explanation based on an analytical model growing out of Powell's work with jet edgetones (38).

TABLE I
Table Summarizing Data From Large Nozzle

	I	II	III	IV	V	VI
	V_0 in./sec.	H in.	Major Spike Frequencies cps	Predicted J-KE Frequencies	Explanation	mf_d
1	1540	5.50	100 245	105 245	J-KE J-KE + Line	$3f_d$ $7f_d$
2	1850	5.50	130 280	126 294	J-KE J-KE + Line	$3f_d$ $7f_d$
3	2170	5.50	150 290	150 350	J-KE J-KE + Line	$3f_d$ $7f_d$
4	2620	5.50	175	180	J-KE	$3f_d$
5	1760	4.31	150 325	153 357	J-KE J-KE + Line	$3f_d$ $7f_d$
6	2240	4.31	200 465	195 455	J-KE J-KE	$3f_d$ $7f_d$
7	2730	4.69	250 500	219 511	J-KE + Line J-KE	$5f_d$ $7f_d$
8	1630	2.44	300 425	252 420	J-KE + Line J-KE	$3f_d$ $5f_d$
9	2350	2.31	400 945	384 896	J-KE J-KE + Line	$3f_d$ $7f_d$
10	2690	2.31	425 780	435 725	J-KE J-KE	$3f_d$ $5f_d$

Fig. 34 shows the results of a series of tests conducted with the geometry of Fig. 30 where:

1. Geometry is made unsymmetrical -- solid line plus circles
2. Geometry is made symmetrical -- dashed line plus circles
3. Geometry is made unsymmetrical, control port open -- dashed line plus stars
4. No knife edge geometry present but an edge inserted at the same position downstream parallel to jet -- solid line plus stars

With the edge parallel to jet, the frequency of the spike changes to a value of $9 f_d$ as predicted by expression (3). Since the source of these oscillations is almost certainly due to an edge tone type feedback loop, the jet knife edge model has limitations similar to those encountered by Powell. When the geometry was made symmetrical, the amplitude of the oscillations decreased. This result may be due to a decrease in feedback flow due to an increase in symmetry.

Further Crosscorrelation Results and Discussion

The waves in Fig. 35 were obtained with probes in the jet when oscillations were present. The

geometry was unsymmetrical as shown in Fig. 30. The measurements were taken with an anemometer probe positioned as follows:

1. Halfway between the knife edge and jet-exit planes
 - a. At the centerline - B
 - b. In the mixing zone on the knife-edge side - A
 - c. In the mixing zone opposite the knife edge side - C
2. On the centerline of the jet parallel to the edge - D

These velocity spectra were taken at the same time as the pressure spectrum shown in Fig. 32. The resonant peaks were only noticeable in the potential core. In the mixing regions and further downstream the inherent turbulent fluctuations of the flow smooth out the spectrum and the resonance tends to lose its identity. The receivers positioned downstream in the typical cases investigated were then excited at their resonant points by the fluctuating flow fields at their entrances. This result confirms the zero cross-correlation obtained digitally.

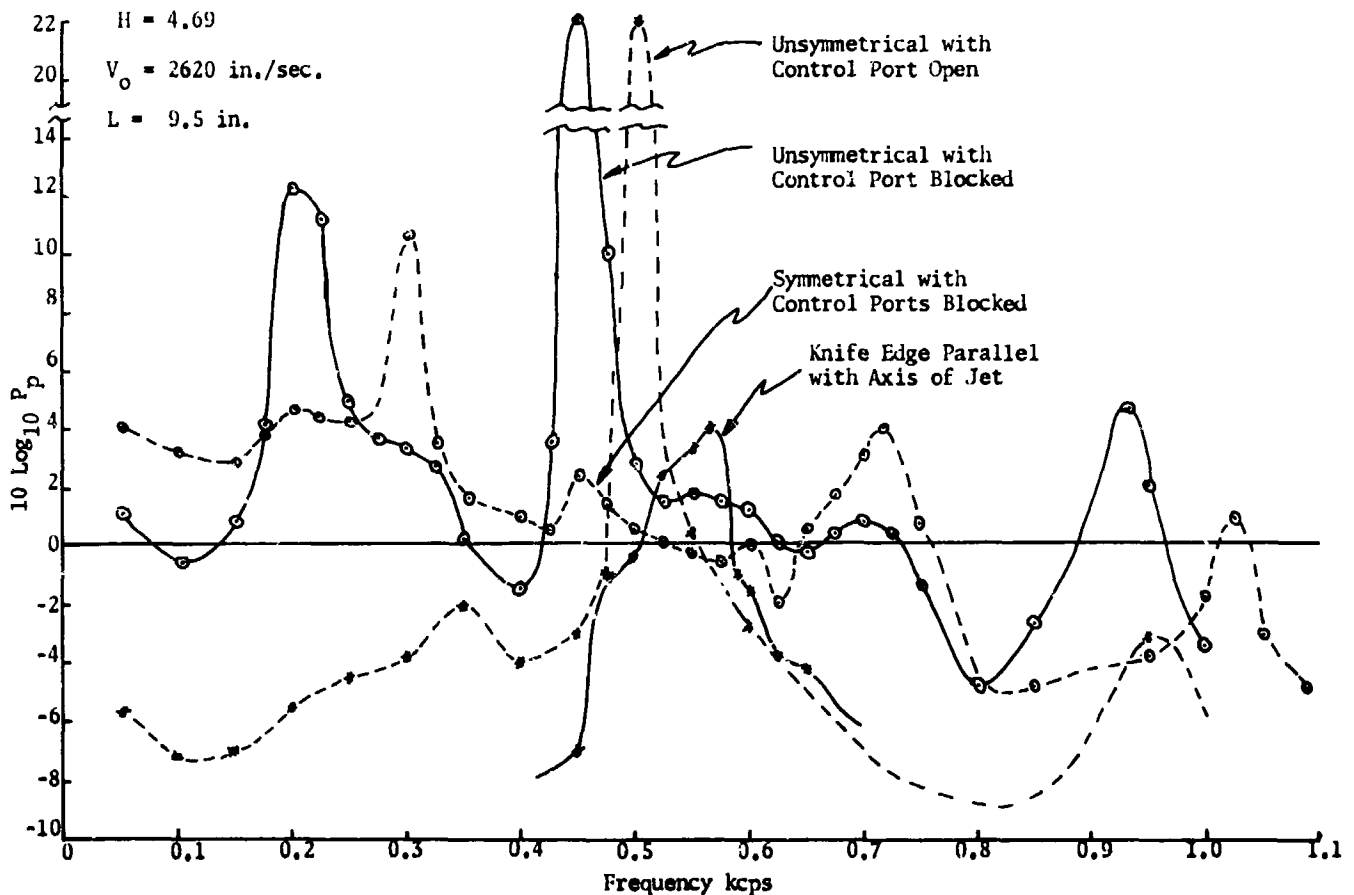


Fig. 34 Power Density Spectrum of Control Port Pressure

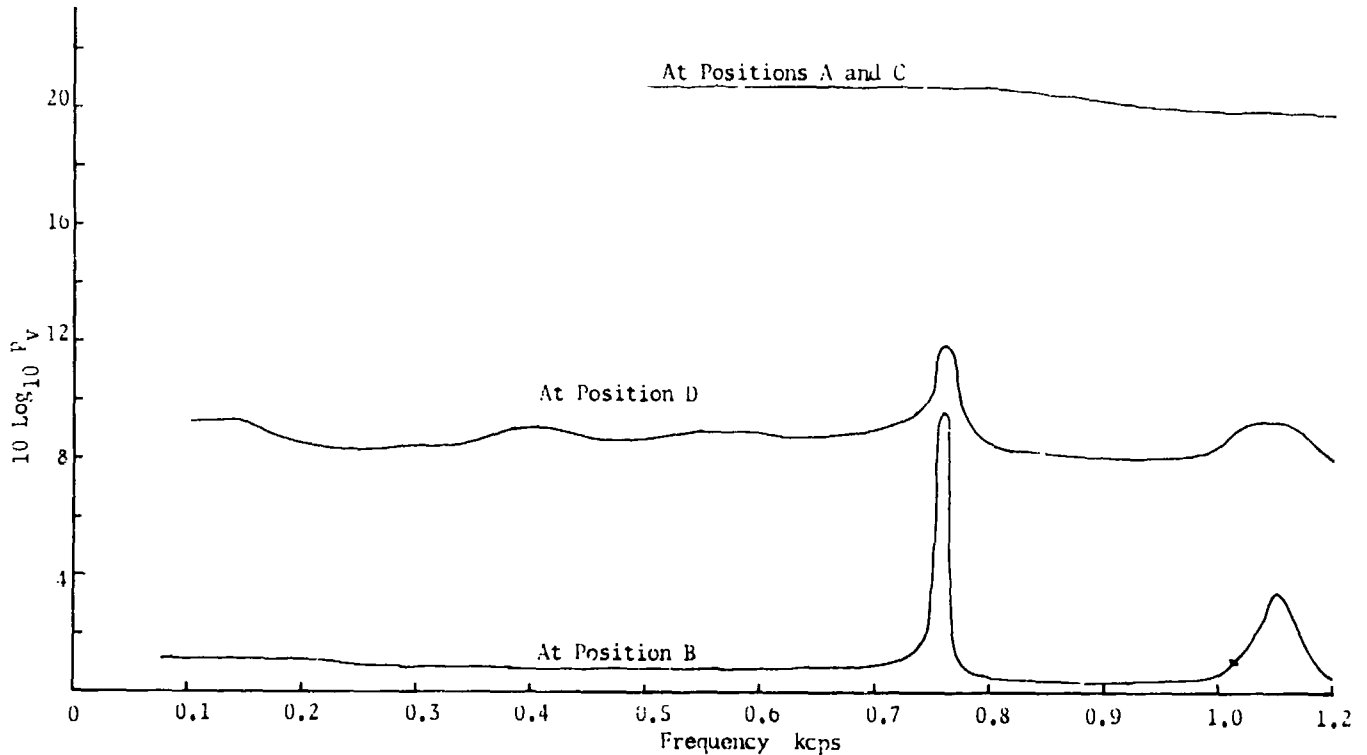


Fig. 35 Power Density of Velocity Fluctuations at Various Positions

Once again using the large model of Fig. 30, the knife edge geometry was made symmetrical and unsymmetrical with two blocked passages positioned ten nozzle diameters downstream in order to stimulate receivers. When the receivers were of a size corresponding to the nozzle area, pressure disturbances measured at the blocked ends had spectra of the form shown by Fig. 25. With passages of equal length, the pressure fluctuations measured at the load end were uncorrelated with each other. With very small area tubes of equal length inserted into the flow field at the same points, the pressure fluctuations measured at the blocked end exhibited appreciable correlation with each other only when the spacing between the tubes was less than a nozzle diameter. With a single receiver positioned on the centerline of the jet, ten nozzle diameters downstream of the nozzle the true RMS value of the pressure fluctuations at the blocked end varied linearly with supply pressure (see Fig. 36). Once again the spectrum of the velocity fluctuations at the entrance had a spectrum indicated by Fig. 26. Fig. 37 is the velocity spectrum at the entrance and Fig. 38 is the pressure spectrum at the load end measured by means of the electronic frequency analyzer. The pressure spikes are given by Eq. (1) and the velocity spectrum indicates an autocorrelation curve of the form shown in Fig. 17 of Research Report No. 3.

The above results confirm the validity of the frequency given in Eq. (1). However, the actual phenomenon is quite complicated. The passages are being driven by the fluctuating flow field at their entrance. Through application of the expressions developed for aerodynamic sound generation, the source terms can be given by a volume integral together with associated surface integrals. While the expression is complex, experimental results show that for the typical length to diameter ratios found in fluid amplifier applications, higher modes can be

neglected. Also, experimental results and application of backscattering techniques outlined in References (40) and (41) indicate that this fluctuating flow field will be a very slow impedance source with respect to the characteristic impedance of the passages. Driving the fluid lines with a source of this type, with the load end blocked, Eq. (1) can be redeveloped. The amplitude of these fluctuations is, however, much more difficult to predict. The interaction of the flow field and geometry is complicated and can be further complicated through feedback to the nozzle. The only positive conclusion which can be made now is that the pressure fluctuations are load

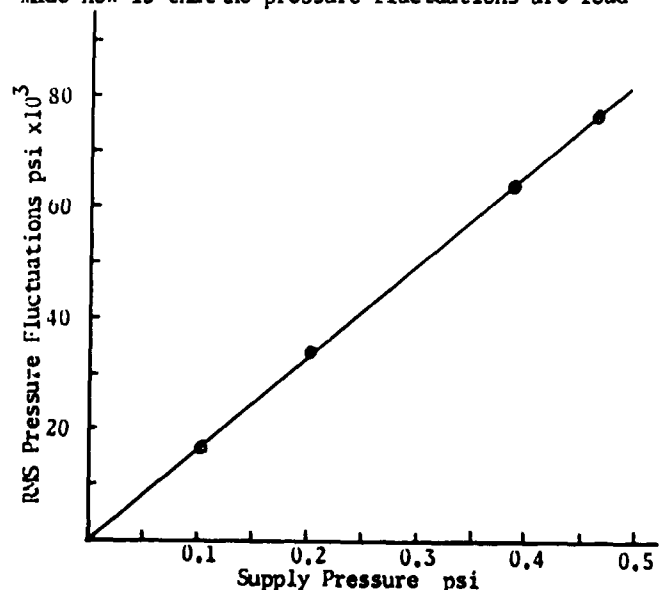


Fig. 36 Pressure Fluctuation at Blocked End Versus Supply Pressure -- Receiver Located 10.0 in. from Nozzle on ϕ

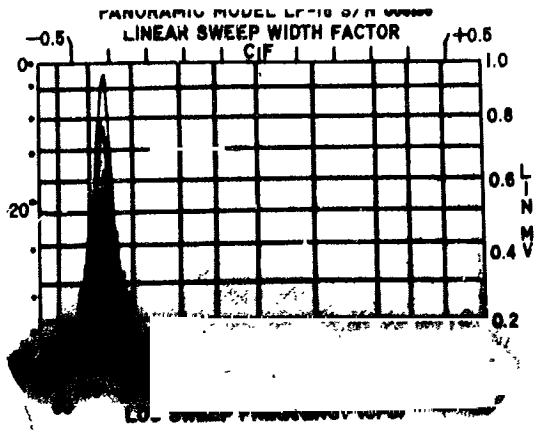


Fig. 37 Average Pressure Envelope - Blocked End

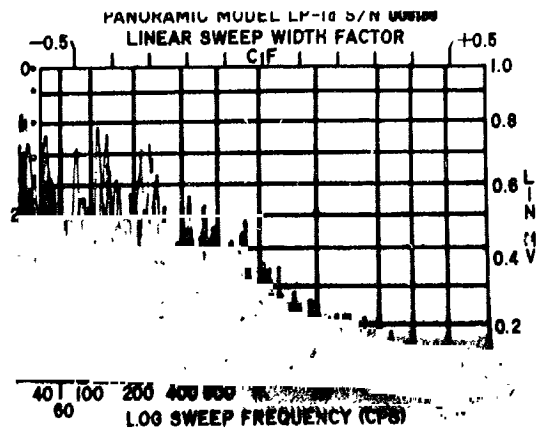


Fig. 38 Average Velocity Envelope - Open End

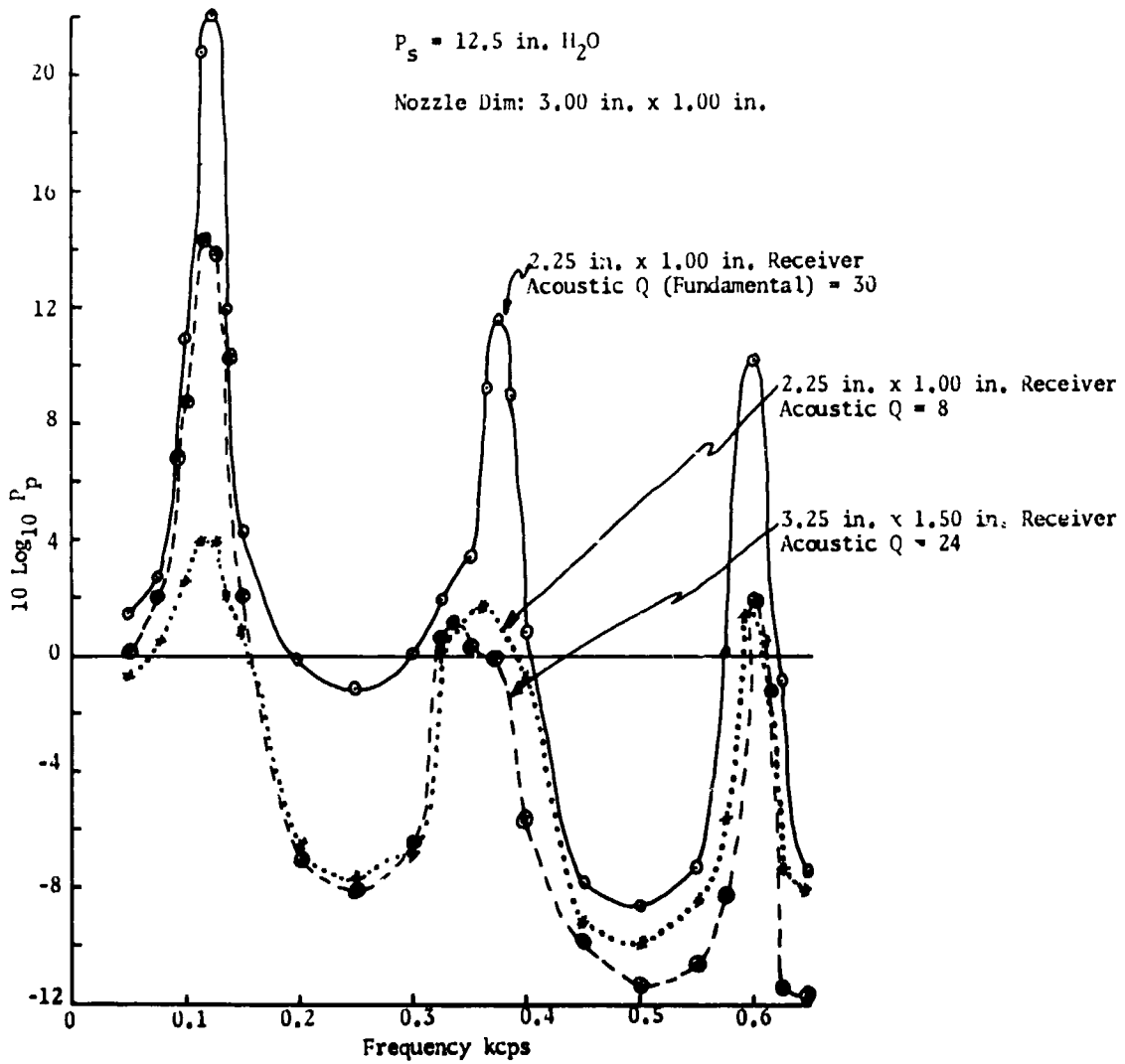


Fig. 39 Power Density Spectrum of Pressure at Blocked End of Receiver on ϕ , 10 in. from Nozzle

sensitive. In particular, the RMS noise could be controlled by adjusting the "Q" of the lines. Fig. 39 shows the result of an experiment with two different size lines. The "Q" of one line was decreased and a corresponding decrease in RMS fluctuations was measured. Besides some applications of transmission line filtering, no further effort was expended in this direction. This course of action was taken since the data taken indicated that pressure fluctuations whose frequency is predictable by application of the principles leading to Eq. (1) and whose amplitude is load sensitive, are generally small as compared to fluctuations that can be excited through jet oscillations. In order to better understand how these oscillations enter into fluid amplifier design, attention was then centered on nozzle design and aspect ratio.

Work recently completed by R. Bettoli and A.K. Stiffler were additional incentives to investigate this area. Stiffler's results show that low aspect amplifiers can have very high gain. One of Bettoli's findings was the existence of a separation bubble present upstream of the nozzle exit point for a certain nozzle-supply chamber design.

Data taken this far indicate that power jets with fluctuations present in the core at the jet exit plane are harder to excite into oscillation. Measurements taken for different configurations confirm that jets, whose core fluctuations with respect to fluctuations at the jet boundary are small, are excited more easily and produce larger pressure fluctuations in the control ports. This appears to be associated with the greater ability of the jet with a relatively quiet core to take small disturbances near the nozzle and to roll these disturbances up into downstream vortices. However, low spatial resolution measurements made in the power jet near the exit plane of a medium-sized nozzle ($d = .375$ in.) did not reveal any measurable effect on the profile due to upstream conditioning (as measured by the intensity of the core velocity fluctuations). Only when profile measurements were made downstream (at least $10 d$), the jets with quieter cores (i.e., larger control port oscillations with knife edge present) were found to have apparently spread more rapidly and to exhibit a more gradual transition (lower peak slope) from centerline velocity to outside edge velocity. Figs. 40 and 41 are results of experiments conducted with a model having an aspect ratio of 5. In this series of experiments, the

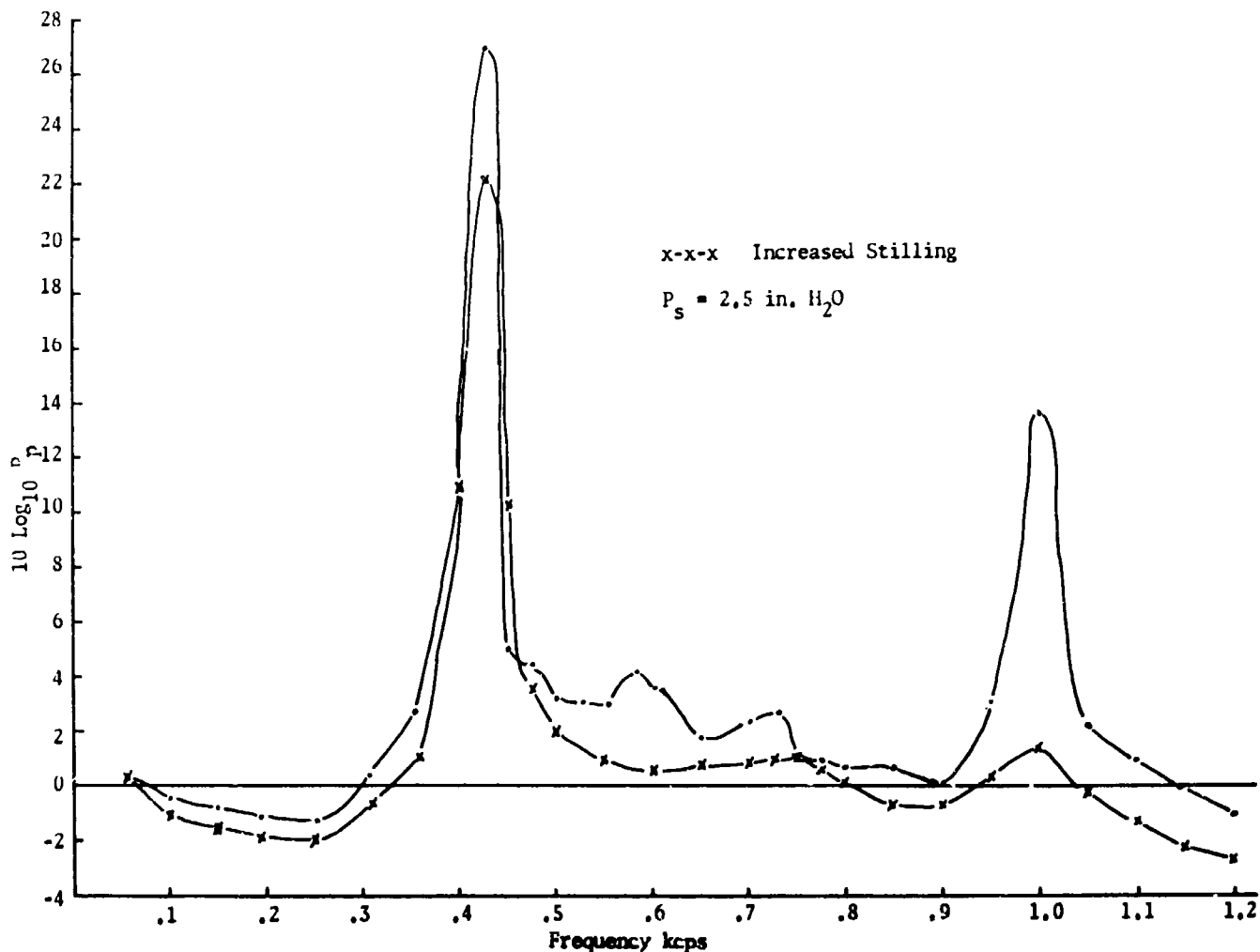


Fig. 40 Power Density Spectrum of Control Port Pressure

geometry and mean jet exit velocity were held constant. The change made was in the supply chamber where for the curves indicated, additional stilling of the flow was introduced. Further work in this area is under way and near completion.

This work is partially supported by NASA Grant NGR 39-009-023.

For further information about the projects mentioned in this report or the activities of the Systems and Controls Laboratory, inquiries should be addressed to: Director, Systems and Controls Laboratory, 214 Mechanical Engineering Building, University Park, Pennsylvania (16802).

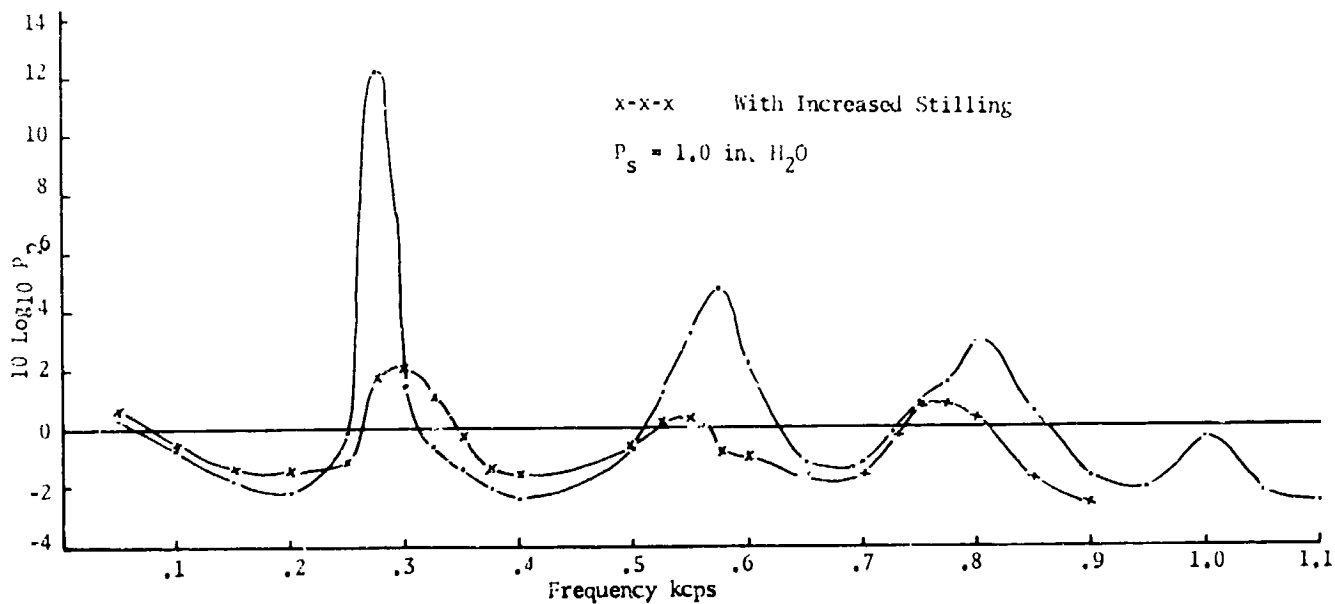


Fig. 41 Power Density Spectrum of Control Port Pressure

LIST OF REFERENCES

1. Research Report No. 1, Systems and Controls Laboratory, The Pennsylvania State University, April 1965.
2. Research Report No. 2, Systems and Controls Laboratory, The Pennsylvania State University, October 1965.
3. Research Report No. 3, Systems and Controls Laboratory, The Pennsylvania State University, April 1966.
4. "Investigations of Effects of Surface Temperature and Single Roughness Elements on Boundary-Layer Transition", H. Leipmann and G. Fila, NACA TN No. 1190, April 1947.
5. "Fluidic Electro-Fluid Converter", D. McGlaughlin and C.K. Taft, Joint Automatic Control Conference, Seattle, Washington, August 18, 1966.
6. Modern Developments in Fluid Dynamics, Vol. I, S. Golstein, Dover Publications, Inc., New York, 1955.
7. "Some Effects of Vanes and of Turbulence in Two-Dimensional Wide Angle Subsonic Diffusers", C.A. Moore, Jr. and S.J. Kline, NACA TN 4060, June 1958.
8. "Performance Characteristics of Plane-Wall Two-Dimensional Diffusers", E.G. Reid, NACA TN 2388, 1953.
9. "An Experimental Investigation of the Flow of Air in a Flat Broadening Channel", A.N. Vedernikoff, NACA TN 1059, 1944.
10. Control of Closed Loop Systems Having Dead Time, H.H. Herritt, M.S. Thesis, The Pennsylvania State University, September 1965.
11. Fluid Power Control, J.F. Blackburn, G. Reethof, and J.L. Shearer, The M.I.T. Press, Massachusetts, and John Wiley and Sons Inc., New York, 1960.
12. "Computer Representative of Engineering Systems Involving Fluid Transients", F.D. Ezekiel and H.M. Paynter, Trans. ASME, Vol. 79, 1840-1850, 1957.
13. "Simplification of Hydraulic Line Dynamics by Use of Infinite Products", R. Oldenburger and R.E. Goodson, Journal of Basic Engineering, Trans. ASME, Series D, Vol. 86, 1-10, 1964.
14. "Performance Measurement of Nonlinear Process Controls", S.A. Steele, Proceedings IEEE, Region III Convention, April 1965.
15. Performance of Third-Order Nonlinear Control Systems, R. Wasta, M.S. Thesis, The Pennsylvania State University, 1966.
16. Theory and Problems of Matrices, Ayres, Schaun Publishing Co., 1962.
17. Analysis of Step Response Error for a Class of Nonlinear Control Systems, S.A. Steele, Ph.D. Thesis, The Pennsylvania State University, March 1965.
18. "A Variable Gradient Method for Generating Liapunov Functions", D. Schultz and J. Gibson, AIEE Transactions, February 1962.
19. "A Method for Minimizing the Number of Internal States in Incompletely Specified Sequential Networks", A. Grasselli and F. Luccio, IEEE Transactions on Electronic Computers, June 1965.
20. "Flow Table Simplification -- Some Useful Aids", S.H. Unger, IEEE Transactions on Electronic Computers, June 1965.
21. Switching Theory, Vol. II, R.E. Miller, John Wiley and Sons, Inc., New York, 1965.
22. Logical Design of Switching Systems, H.C. Torng, Addison Wesley Publishing Co., Massachusetts, 1964.
23. Introduction to the Theory of Switching Circuits, E.J. McCluskey, McGraw-Hill Book Co., Inc., New York, 1965.
24. "A Technique for the Reduction of a Given Machine to a Minimal State Machine", S. Ginsburg, IRE Transactions on Electronic Computers, Vol. EC-8, No. 3, September 1959.
25. See portion of Reference 1, by R.S. Raizada, entitled "Hysteretic Nonlinearities in Closed Loop Control Systems".
26. A Root Excursion Method of Nonlinear Qualitative Analysis, C. Volz, Ph.D. Thesis, The Pennsylvania State University, 1958.
27. Mathematical Theory of Compressible Fluid Flow, R. Von Mises, Academic Press, Inc., New York.
28. "Flow of Compressible Fluid Through Orifices", D.A. Jobson, Proc. Inst. Mech. Engs., Vol. 169, London, 1955.
29. "The Effect of Compressibility on the Discharge Coefficients of Orifices and Convergent Nozzles", S.L. Bragg, Journal Mech. Eng. Sci., Vol. 2, 1960.
30. A Study of Jet Flow and Reattachment in Control Valves, R.D. Begg, Ph.D. Thesis, University of Glasgow, Scotland, 1965.
31. "Gain Characteristics of Subsonic Pressure-Controlled, Proportional, Fluid Jet Amplifiers", A.K. Simson, ASME Trans., Journal of Basic Engineering, 1965.
32. "Static Characteristics of a Pressure-Controlled Jet Fluid Amplifier for Low Aspect Ratio and High Velocity Jets", A.K. Stiffler, Special Summer Course on Fluid Power Control, Massachusetts Institute of Technology, July 1966.
33. "Static Characteristics and Staging Possibilities of Pressure-Controlled Jet Fluid Amplifiers with Low Aspect Ratios", A.K. Stiffler, National Conference on Fluid Power, October 1966.

34. "Development of Techniques for the Static and Dynamic Analysis of Fluid State Components and Systems", C.A. Belsterling, USAAVLABS Technical Report 66-16, U.S. Army Aviation Material Laboratories, February 1966.
35. "A Lumped-Parameter Technique for Predicting Analog Fluid Amplifier Dynamics", W.A. Boothe, ISA Trans., Vol. 4, No. 1, January 1965.
36. Static and Dynamic Modeling of a Pressure-Controlled Subsonic Fluid Jet Modulator, R.J. Gurski, Sc.D. Thesis, Department of Mechanical Engineering, Massachusetts Institute of Technology, May 1965.
37. "Self-Maintained Oscillation of the Jet in a Jet Edge Stream", W.L. Nyborg, Journal of the Acoustical Society of America, Vol. 26, March 1954.
38. "On the Edgetone", A. Powell, Journal of the Acoustical Society of America, Vol. 33, April 1961.
39. "The Mechanics of Edgetones", N. Curle, Proceedings of the Royal Society, London, 216A, 412-424, 1953.
40. "Scattering Theory for One-Dimensional Problems", M. Harrison and R. Plutchok, JASA, Vol. 37, 84-89, January 1965.
41. "Scattering Theory with Applications to One-Dimensional Problems", M. Harrison and R. Plutchok, JASA, Vol. 37, 1056-1062, June 1965.
42. The Theory of Sound, Vol. II, J.W.S. Rayleigh, Dover Publications, Inc., New York, p. 202, 1945.